TECHNICAL RESEARCH REPORT

Modeling and Optimization for Epitaxial Growth: Transport and Growth Studies

by Andrew J. Newman, P.S. Krishnaprasad

CDCSS T.R. 99-2
(ISR T.R. 99-19)

The Center for Dynamics and Control of Smart Structures (CDCSS) is a joint Harvard University, Boston University, University of Maryland center, supported by the Army Research Office under the ODDR&E MURI97 Program Grant No. DAAG55-97-1-0114 (through Harvard University). This document is a technical report in the CDCSS series originating at the University of Maryland.

Web site http://www.isr.umd.edu/CDCSS/cdcss.html

Report Documentation Page

Form Approved
OMB No. 0704-0188

1. REPORT DATE	2. REPORT TYPE	3. DATES COVERED
1999		**-**

4. TITLE AND SUBTITLE	5a. CONTRACT NUMBER
Modeling and Optimization for Epitaxial Growth: Transport and Growth Studies	5b. GRANT NUMBER
	5c. PROGRAM ELEMENT NUMBER
6. AUTHOR(S)	5d. PROJECT NUMBER
	5e. TASK NUMBER
	5f. WORK UNIT NUMBER
7. PERFORMING ORGANIZATION NAME(S) AND ADDRESS(ES) **Army Research Office,PO Box 12211,Research Triangle Park,NC,27709**	8. PERFORMING ORGANIZATION REPORT NUMBER
9. SPONSORING/MONITORING AGENCY NAME(S) AND ADDRESS(ES)	10. SPONSOR/MONITOR'S ACRONYM(S)
	11. SPONSOR/MONITOR'S REPORT NUMBER(S)

12. DISTRIBUTION/AVAILABILITY STATEMENT
Approved for public release; distribution unlimited

13. SUPPLEMENTARY NOTES
The original document contains color images.

14. ABSTRACT
see report

15. SUBJECT TERMS

16. SECURITY CLASSIFICATION OF:			17. LIMITATION OF ABSTRACT	18. NUMBER OF PAGES	19a. NAME OF RESPONSIBLE PERSON
a. REPORT	b. ABSTRACT	c. THIS PAGE			
unclassified	**unclassified**	**unclassified**		**40**	

Modeling and Optimization for Epitaxial Growth: Transport and Growth Studies

Andrew J. Newman *
Institute for Systems Research and
Electrical Engineering Department
University of Maryland
College Park, MD 20742
newman@isr.umd.edu

P. S. Krishnaprasad
Institute for Systems Research and
Electrical Engineering Department
University of Maryland
College Park, MD 20742
krishna@isr.umd.edu

Original Version: January 10, 1999
Current Version: March 17, 1999

Abstract

This report details the objectives, methodologies, and results for Phase II of the project, "Modeling and Optimization for Epitaxial Growth" (see [21] for Phase I report). This project is a joint effort between the Institute for Systems Research (ISR) and Northrop Grumman Corporation's Electronic Sensors and Systems Sector (ESSS), Baltimore, MD. The overall objective is to improve manufacturing effectiveness for epitaxial growth of silicon and silicon-germanium (Si-Ge) thin films on a silicon wafer. Growth takes place in the ASM Epsilon-1 chemical vapor deposition (CVD) reactor, a production tool currently in use at ESSS. Phase II project results include development of a new comprehensive process-equipment model capable of predicting gas flow, heat transfer, species transport, and chemical mechanisms in the reactor under a variety of process conditions and equipment settings. Applications of the model include prediction and control of deposition rate and thickness uniformity; studying sensitivity of deposition rate to process settings such as temperature, pressure, and flow rates; and reducing the use of consumables via purge flow optimization. The implications of various simulation results are discussed in terms of how they can be used to reduce costs and improve product quality, e.g., thickness uniformity of thin films. We demonstrate that achieving deposition uniformity requires some degree of temperature non-uniformity to compensate for the effects of other phenomena such as reactant depletion, gas heating and gas phase reactions, thermal diffusion of species, and flow patterns.

*This research was supported by grants from the Northrop Grumman Foundation, the National Science Foundation's Engineering Research Centers Program: NSFD CDR 8803012 and NSF Grant EEC-9527576, and the Army Research Office under the ODDR&E MURI97 Program Grant No. DAAG55-97-1-0114.

Contents

1 Introduction

This report details the objectives, methodologies, and results for Phase II (covering March 1998 through February 1999) of the project, "Modeling and Optimization for Epitaxial Growth" (see [21] for Phase I report). This project is a joint effort between the Institute for Systems Research (ISR) and Northrop Grumman Corporation's Electronic Sensors and Systems Sector (ESSS), Baltimore, MD. The overall objective is to improve manufacturing effectiveness for epitaxial growth of silicon and silicon-germanium (Si-Ge) thin films on a silicon wafer. Growth takes place in the ASM Epsilon-1 chemical vapor deposition (CVD) reactor, a production tool currently in use at ESSS. Phase II project results include development of a new comprehensive process-equipment model capable of predicting gas flow, heat transfer, species transport, and chemical mechanisms in the reactor under a variety of process conditions and equipment settings. Applications of the model include prediction and control of deposition rate and thickness uniformity; studying sensitivity of deposition rate to process settings such as temperature, pressure, and flow rates; and reducing the use of consumables via purge flow optimization. The implications of various simulation results are discussed in terms of how they can be used to reduce costs and improve product quality, e.g., thickness uniformity of thin films. We demonstrate that achieving deposition uniformity requires some degree of temperature non-uniformity to compensate for the effects of other phenomena such as reactant depletion, gas heating and gas phase reactions, thermal diffusion of species, and flow patterns.

The Epsilon-1 is a single-wafer lamp-heated CVD reactor manufactured by ASM, Inc., Phoenix, AZ. The reactor is used for depositing layers of epitaxial Si-Ge, epitaxial silicon (epi-Si), and polycrystalline silicon (poly-Si). Initial physical-mathematical models for growth of polycrystalline silicon in the Epsilon-1 are presented in [21]. The initial models focus on thermally activated growth of poly-Si in the Epsilon-1. They incorporate heat transfer within the wafer and between wafer, chamber walls, and lamps; and surface deposition chemical kinetics. Experimental validation of lamp heating models and experimental determination of chemical kinetics parameters are also presented. However, the initial models suffer from some deficiencies which we now discuss.

The modeling of fundamental aspects of CVD involves both chemical kinetics and transport phenomena. Depending on the specific process and operating conditions, it is often assumed that one or more factors has significantly more influence than all others over deposition product. In those cases, the factors that are considered less important are often completely or mostly neglected.

This type of simplification was adopted in the initial models, which focused on low temperature epitaxy. In the low temperature regime, growth rate is limited by surface reaction phenomena rather than by mass transport phenomena. Furthermore, surface reaction phenomena such as adsorption and desorption of reactant species are strongly dependent on temperature. For this reason, the low temperature regime is said to be thermally driven (kinetically limited). This motivated an approach in which initial models consisted only of a simplified conjugate heat transfer model and an Arrhenius growth law. Dynamics of transport phenomena were neglected. Inlet conditions for gas phase species concentrations and temperature were assumed to hold throughout the process chamber. Chamber geometry played no role.

However, as we show in this report, the simplifications made for the initial models seriously compromise their usefulness toward studying uniformity issues for thin film growth in the Epsilon-1. It turns out that chamber geometry and a variety of complex phenomena play a role, including depletion of reactants, non-uniform gas heating, gas phase chemistry, thermal diffusion, and gas flow patterns. This necessitates the incorporation of detailed models for three-dimensional effects of gas flow, gas phase heat transfer, and transport of chemical species, in addition to the previously modeled heat transfer phenomena. Furthermore, a more accurate model for surface reaction chemical kinetics is required to incorporate reactive intermediaries produced in the gas phase. Finally, it is crucial that the models reflect the coupling among these various phenomena in the process chamber.

Deficiencies in the initial models have been addressed by development of a comprehensive process-equipment model which accounts for the mechanisms and factors described above. The model provides a platform for studying the effect of equipment settings and process conditions on deposition product characteristics, e.g., deposition rate and thickness uniformity.

This report is organized as follows. Section 2 serves as a stand-alone executive project summary and general overview of results. Section 3 provides details of the equipment and processes on which the models are based. The comprehensive process-equipment model is presented in Section 4. Results and applications of the modeling effort are contained in Section 5. We give some concluding remarks in Section 6.

2 Project Summary

This section serves as a stand-alone executive summary. It summarizes project objectives and results from the viewpoint of benefits to semiconductor manufacturing at Northrop Grumman.

2.1 Objectives

As stated earlier, the overall objective of the project is to improve manufacturing effectiveness for growth of thin films in the Epsilon-1 reactor. The overall goal is accomplished via improvement of product quality, increased flexibility of operation, and reduction of manufacturing costs. The description of project objectives and process details that follows is based on discussions with and demonstrations by Northrop Grumman participants [23].

Within the scope of this phase of the project, product quality is determined solely by deposition thickness uniformity. Other factors, such as film composition and resistivity uniformity, are important quality measures but not considered here. Thickness variations of 5% are currently acceptable for most applications, although there is no guarantee that such a specification will remain stable. Currently, variations in the range of 2% are routinely achieved with the Epsilon-1. Improved results are always desirable.

The Epsilon-1 is capable of operation in several regimes for pressure, temperature, and flow rates, and deposition via injection of several types of precursor and carrier gases. Prediction of deposition rates and other film characteristics for a given combination of process conditions is key to taking advantage of the machine's flexibility. The manufacturer provides some predictive guidance and data. However, there is the desire for manufacturing "off-the-curve," i.e., operating in regimes and producing films with characteristics that do not appear in manufacturer provided information.

We have identified and focused on several manufacturing costs for which reduction would be advantageous. Performance of devices at high frequency is difficult to predict based on properties of the product and manufacturing parameters. To achieve a product with the desired properties, Northrop Grumman operates with a three to four month manufacturing cycle followed by a long testing cycle. It can take up to two years to converge on the desired product. Each manufacturing cycle requires an initial period of experimentation in which the necessary equipment settings and process conditions are determined. Once parameters are determined, and the customer is satisfied, the process is certified, and parameters are usually not changed for several years in order to provide the customer with a consistent product. It is possible, however, for drift of equipment characteristics over time to causes degradation, necessitating additional experimentation. In addition, the chamber tube is periodically cleaned and replaced, requiring a re-calibration of process settings. The result is that the various trial-and-error steps have a significant impact on time-to-manufacture and other production costs.

Other cost concerns include operational integrity and "down-time" of equipment, and the use of consumables such as process gases. It is clear that reductions in experimental steps, equipment failure, and gas consumption will have a beneficial impact on manufacturing costs.

2.2 Methodology

Project objectives are accomplished by

- gaining an understanding of the processes and equipment via physical and mathematical modeling, and
- using the resulting validated models for optimization of process conditions and equipment settings.

The modeling effort includes development of physics based models for fundamental CVD phenomena, experimental determination of modeling parameters, and experimental validation of model predictions. Process and equipment models are used to develop software and analytical tools for "off-line" prediction of deposition results, conducting "what-if" experiments, and determining operating parameters for improved performance and product quality.

2.3 History

The project "Modeling and Optimization for Epitaxial Growth" was initiated in December 1996, under an agreement between Northrop Grumman ESSS and the ISR. Phase I of the project roughly encompassed the period January 1997 through September 1997. Final Phase I results were presented to Northrop Grumman participants in August 1997, at the SEMATECH Advanced Equipment/Process Control Symposium [20] in September 1997, and published in [21].

Phase II of the project began in March 1998. A formal presentation of results to Northrop Grumman participants was made in October 1998. This report, which includes some additional results, and revisions to the October 1998 presentation, was written during the subsequent period.

2.4 Summary of Phase I Results

There are two main components of the Phase I effort [21]: physics based modeling of poly-Si growth in the Epsilon-1 and a comparative study of methods for reducing the complexity of those models so they are easier to use for simulation and control purposes.

The initial modeling effort produced a detailed analysis of physical and chemical mechanisms for growth in the Epsilon-1, along with an overall modeling framework which identified and integrated the necessary model components such as macroscopic level heat transfer and microscopic level morphology evolution. Then, simplified physics based models for poly-Si deposition in the Epsilon-1 were developed. These models predict the time evolution for

- heat transfer within the wafer and among wafer, heat lamps, and chamber walls (temperature distributions in solids), and
- reaction rate at the wafer surface via chemical kinetics.

The initial wafer thermal model accounts for effects of conduction within the solid wafer, convective losses to the gas phase, and radiative losses to the ambient. Radiative heat transfer from lamps to wafer is modeled by determining spatial profiles of radiant heat flux intensity for individual lamp groups and lamp zones. These radiant intensity profiles were computed analytically using viewfactor methods and then validated using data from poly-Si growth experiments using the Epsilon-1 reactor.

The initial chemical kinetics model is an Arrhenius relationship for surface reaction rate versus temperature. The Arrhenius parameters, activation energy and pre-exponential constant, were determined via poly-Si growth experiments using the Epsilon-1 reactor.

The initial models were used to predict growth rates and thickness profiles for several test process recipes. It should be emphasized that the predictive capability of the initial models was limited to the low temperature thermally activated regime. They do not account for the effects of gas flow patterns, gas phase heat transfer, gas phase chemical reactions, and other phenomena affecting the rate and spatial distribution of transport of chemical species to the wafer surface.

Due to the complexity and high computational demands of CVD models, we investigated the use of model reduction techniques to reduce the model complexity, leading to faster simulation and facilitating the use of standard control and optimization strategies. The comparative study of model reduction methods examined the proper orthogonal decomposition (POD) and balanced realization approaches to reducing model complexity. These methods were applied to the dynamic models for heat transfer involving the wafer and lamps in the Epsilon-1. Numerical simulations and subsequent analysis revealed that both the POD and balancing methods produce a state space basis that allows for a significant reduction in model dimensionality (see also [22]).

2.5 Summary of Phase II Results

We developed a comprehensive process-equipment model, incorporating three-dimensional effects of gas flow, heat transfer, species transport, and gas phase and surface chemical mechanisms. The process-equipment model is improved over initial models, in that it is based on more accurate information provided by the manufacturer, and has the capability to take into account more phenomena suspected to have a significant influence on deposition rate and uniformity.

The process-equipment model provides a tool for prediction of deposition rate and other process variables given a set of process conditions and equipment settings. These predictions allow Northrop Grumman to simulate growth experiments in advance, narrow parameter choices, and perform fewer actual experiments. Conditions and settings can be optimized off-line, taking into account simulation results and sensitivity analysis for pressure, temperature, and flow rates. The effect of adjustments to wafer temperature set-point, chamber pressure, source gas flow rate, thermocouple offsets, and injector settings can be predicted and tuned off-line.

We validated the predictive capability of the model over a range of operating conditions by comparing simulation results with experimental data. We used simulations to predict the relationship between silicon growth rate and wafer temperature, chamber pressure, source gas flow rate, and choice of carrier gas. We determined an Arrhenius

relationship for temperature sensitivity of silicon growth rate, with activation energy the same for simulations and experiments. Simulation results indicate that growth rate increases with the logarithm (base 10) of chamber pressure, in agreement with known relationships. We found a power law relationship connecting poly-Si growth rate with silane flow rate at the inlet. Finally, we demonstrated that substitution of nitrogen for hydrogen as the carrier gas results in a significantly increased deposition rate.

We show in this report that a uniform temperature distribution on the wafer surface results in a non-uniform deposition thickness profile. Thus, it is apparent that achieving deposition uniformity requires some degree of temperature non-uniformity to compensate for the effects of other phenomena. This temperature non-uniformity is provided by the thermocouple offsets. The factors that influence deposition rate and uniformity are studied with the goal of formulating strategies for the setting of thermocouple offsets.

Simulation results show that consumption of process gases can be reduced by decreasing the purge gas flow from 7 slm to 5 slm and possibly further without compromising the ability of the purge gas to prevent back-side deposition.

2.6 Follow-On Plans

Existing gas injection equipment in the Epsilon-1 will be replaced in the near future with new gas injectors. The new equipment will provide more degrees of freedom for adjusting the gas flow profile in the process chamber. The models should be revised to reflect the new equipment, and the effect of varying injector opening sizes should be investigated via simulations and experiments.

It is clear that the setting of thermocouple offsets has a strong influence on deposition uniformity in the Epsilon-1. An experimental study is necessary to investigate the effect of each individual offset on wafer temperature distribution and growth rate uniformity.

Northrop Grumman has observed that a build-up of deposited material leaves a coating on the quartz shelves [23]. The effect on deposition uniformity is unclear, although it has not yet caused a problem in that regard. Its main damage is to the structural integrity of the chamber. In one instance, mechanical stresses due to film build-up on the quartz caused the quartz to crack, destroying the chamber. For this reason, the quartz chamber is cleaned or replaced periodically. In addition, the flow guide has been used to direct the flow so that the build-up occurs in a less damaging location.

In order to prevent unwanted build-up of films, an etch clean step using HCl is performed prior to deposition steps. During this step, HCl is pumped into the chamber along with H_2 purge gases. It is possible that the flow of purge gases through the ring-shelf gap forces the etch gas away from certain locations on the shelf near the gap, thus preventing etching in those locations. A reduction in purge gas flow rate may alleviate this occurrence. The effect of purge gas flow on the HCl etch clean of the chamber should be studied via simulation with the goal of reducing the buildup of deposits on chamber walls.

Models for Si-Ge chemical mechanisms are needed to apply the process-equipment model to Si-Ge growth. ISR participants are receiving assistance from a government laboratory [19] toward determining chemical kinetics parameters for growth of Si-Ge.

Northrop Grumman is interested in thin film growth on patterned wafers. It is necessary to study the effect of flow and thermal conditions on film morphology for patterned wafers, and to determine the relationships among pattern pitch, thickness uniformity, and process conditions.

3 Equipment and Product

The ASM Epsilon-1 reactor is a radiantly heated, gas injected, single wafer processing system for CVD of doped or undoped epitaxial layers on a 6 inch diameter semiconductor wafer. Accurate and detailed data regarding the reactor geometry, materials, and operation was furnished by the manufacturer, ASM America, Inc., during an April 1998 visit by the authors to their headquarters and manufacturing facility in Phoenix, AZ.

3.1 Process Chamber

Figure 1 shows a cross-sectional view of the ASM Epsilon-1 process chamber and lamp assembly. Figure 2 shows a top-down view of the wafer level apparatus. Diagrams of other views of the reactor are found in [21]. The inlet and outlet sides of the reactor are referred to as the front and rear, respectively.

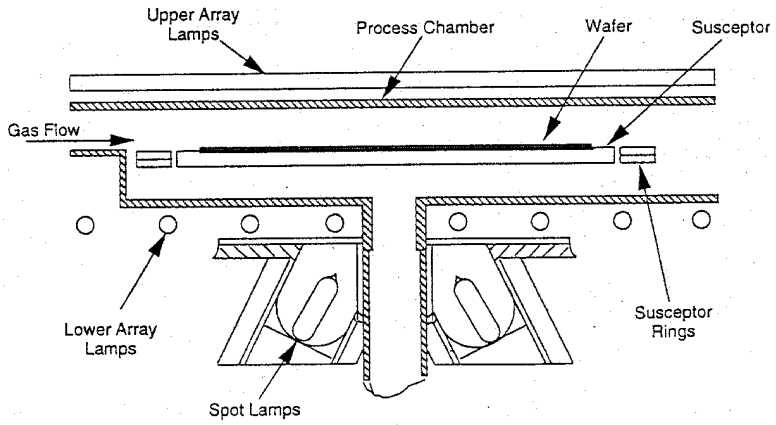

Figure 1: Cross-sectional view of the ASM Epsilon-1 process chamber and lamp assembly. Process gases flow through upper section (above wafer) from inlet (left) to outlet (right). Purge gases flow in lower section (below wafer). The upper lamp array illuminates the top surface of the wafer. The lower lamp array and spot lamps illuminate the bottom of the susceptor.

Deposition takes place in the process chamber, which is a horizontally oriented quartz tube of lenticular shape, i.e., a cross-sectional view looking into the chamber front shows a flat bottom, short vertical sides, and curved top. Process gases are pumped into the chamber through the inlet flange, flow horizontally through the chamber over the wafer surface, and are pumped out through the exhaust flange via pneumatic actuators. An optional flow guide can be used to force the inlet flow away from the chamber roof and toward the wafer. The inlet flange is designed to create a specialized sonic flow with possible swirling and mixing properties as the gas enters the process chamber. It has been observed by the manufacturer that the inlet flange design aids in achieving deposition uniformity [18].

The 6 inch diameter wafer rests on small quartz pins attached to the pocket of a rotating susceptor that is surrounded by the susceptor ring. The susceptor and ring are constructed of graphite coated with silicon-carbide. The chamber is divided by the susceptor, ring, and a quartz shelf into upper and lower sections. Thin gaps between the quartz shelf and the ring, and between the ring and susceptor, allow gas to flow between upper and lower chamber sections. In addition, diffusion of species from upper to lower and visa-versa can occur due to concentration and thermal gradients. For this reason, purge gases are pumped into the lower region through the susceptor rotation shaft and a purge inlet in the front wall. The purge flow prevents the process gases from escaping to the lower section, which can result in unwanted deposition on the back-side of the susceptor.

The wafer and chamber are heated by upper and lower arrays of linear tungsten-halogen lamps, and four spot lamps directed at the center of the susceptor (see [21] for details and analysis). Heat radiation is intensified by gold coated reflectors surrounding the process chamber on all sides. Four thermocouples measure the temperature at the center, front, rear, and side of the susceptor. We note that the while the center thermocouple is located at the center of the susceptor, the other three thermocouples are located at the front, rear, and side of the ring that surrounds the susceptor. Thus, susceptor temperature is measured only approximately at points other than the center.

The quartz chamber and lamp-house are cooled by air flow. All components are contained in a stainless steel enclosure.

3.2 Product and Consumables

Northrop Grumman uses the ASM Epsilon-1 reactor to deposit thin films of epitaxial Si-Ge, epi-Si, and poly-Si. Epitaxial layers are deposited on silicon wafers that are either bare or covered with a patterned layer of silicon dioxide (SiO_2). Poly-Si is deposited on a layer of silicon dioxide.

The major source gases used to deposit epi-Si layers commercially are (see, e.g., [24, 28])

- silane (SiH_4) at low temperatures (< 1000 C); and
- silicon tetrachloride ($SiCl_4$), dichlorosilane (SiH_2Cl_2), and trichlorosilane ($SiHCl_3$) at higher temperatures.

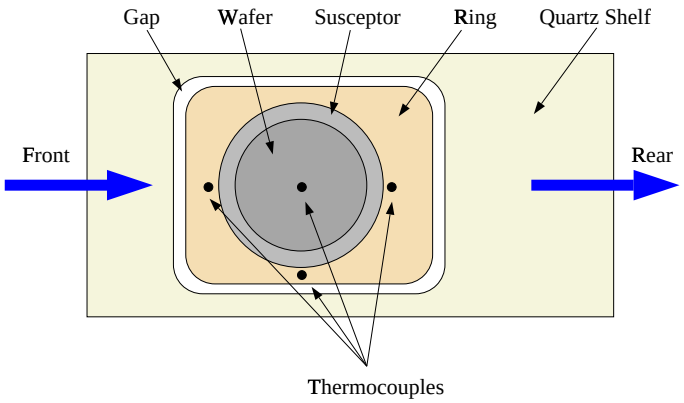

Figure 2: Overhead view of the Epsilon-1 at wafer level. Gas flows from front (upstream) to rear (downstream). The quartz shelves are connected to the quartz chamber walls to form a contiguous body. The graphite coated susceptor ring fits into a space within the quartz structure, leaving a thin gap between ring and shelf on all sides. The graphite coated susceptor fits into the ring structure, and is supported and rotated by special apparatus located through and under the lower chamber section. There is also a gap, although much smaller, between the ring and susceptor. The wafer rests on small quartz pins attached to the susceptor. The center thermocouple measures temperature at the center of the susceptor. The front, rear, and side thermocouples measure temperature at three locations in the ring.

This project deals with low temperature growth, for which Northrop Grumman uses silane as the source gas. Germane (GeH_4) is added to the mixture for growth of Si-Ge. The carrier gas is either hydrogen (H_2) or nitrogen (N_2). Dopant precursors such as arsine (ArH_3) can also be added to the mixture.

There is a direct relationship between growth of poly-Si and epi-Si. The processing steps are identical, and growth rates are virtually identical [23]. Experiments are performed at Northrop Grumman by depositing poly-Si rather than epi-Si, because they have tools for measuring poly-Si films (e.g., nanospec, ellipsometer) but not for epi-Si (e.g., SIMS). (It is the presence of the oxide boundary that allows for easier measurement of poly-Si.) Thus, poly-Si experiments allow for rapid process evaluation. For this reason, Northrop Grumman sometimes performs epi-Si and poly-Si experiments in parallel, with measurements taken for the poly-Si films.

In light of the above, for purposes of this report, we performed experiments and simulations for growth of poly-Si. The process gases used were a mixture of 2% SiH_4 diluted in H_2 as the silicon source, together with 20 slm H_2 as the carrier, except as noted otherwise.

Specifications for the final product (thin film) include characteristics such as chemical composition, film thickness, dopant concentration, crystal structure, resistivity, and possibly other factors. Both aggregate and spatially distributed quantities are important. Usually, spatial uniformity is specified by a variation tolerance across the wafer surface, e.g., 5% allowable non-uniformity.

In general, aggregate characteristics such as average growth rate are determined by process conditions for temperature, pressure, and flow rates as set by the user in process recipes. The spatial distributions of the various properties, and hence uniformity, are mainly controlled by equipment settings such as thermocouple offsets and injector opening sizes. These two methods of equipment and process control are described below.

3.3 Process Conditions and Recipes

In order to achieve the desired aggregate characteristics, the process engineer designs step-by-step recipes. Each step performs a particular task such as etch, bake, purge, or deposit, for a specified amount of time. We consider only the deposition steps here. The process engineer specifies the choice of source, carrier, and purge gases, set-points for temperature, pressure, and flow rates, and time duration, for each deposition step. We refer to these specifications as *recipe inputs*. They are programmed into the Epsilon-1 microprocessor and controlled automatically in–situ. For example, PID controllers and MFCs regulate the thermocouple temperatures and inlet flow rates around their respective set-points.

Si-Ge films are deposited at a temperature of 675 C. This falls within the low temperature regime which is roughly 600–800 C. At low temperature, surface reactions are thermally activated and controlled by deposition ki-

netics. Northrop Grumman also deposits some films in the high temperature regime which is roughly 900–1100 C. At high temperature, surface reactions are mass transport controlled. However, temperature regulation is still important, as it determines layer resistivity, and large temperature gradients can cause slip, i.e., mechanical damage to the wafer. All growth data in this report is restricted to the low temperature regime.

The ASM Epsilon-1 reactor is capable of growth at atmospheric pressure (AP) and reduced pressure (RP) which is roughly 10–100 Torr. For this project, we performed deposition in the RP regime at 20 Torr and 40 Torr. The flow rate for each individual process and purge gas used is specified in standard liters per minute (slm) or standard cubic centimeters per minute (sccm). The process gases, e.g., hydrogen carrier and silane source, are mixed prior to injection into the chamber. The purge flow rate is set to prevent mixing between upper and lower chamber sections, and is generally the same for each recipe. Since its impact is on equipment integrity rather than product characteristics, we treat it separately from the other recipe inputs.

3.4 Equipment Settings

Reactor operation can be adjusted ex-situ via several mechanisms that are included in certain components of the reactor. The process engineer can set the size of gas injector openings in the inlet flange, the relative power setting for each lamp group, PID feedback gains, susceptor rotation rate, and thermocouple offsets. We refer to these as *equipment settings*. In contrast to recipe inputs, the equipment settings are semi-permanent, i.e., they are not changed, in general, for each different process recipe. Rather, once an equipment setting is adjusted so that the reactor yields acceptable films, it remains fixed from run to run until process drift or tube replacement necessitates an adjustment. The equipment settings play a key role in achieving spatial uniformity of deposition thickness in the Epsilon-1. We elaborate on some of these settings here.

As stated earlier, wafer temperature is set as a recipe input. However, this one setting does not provide the capability to adjust the temperature distribution across the wafer surface. The necessary additional degrees of freedom are provided by the thermocouple offsets. There are three offsets, one each for thermocouples at the front, rear, and side of the susceptor. The center thermocouple has no offset, and its temperature is regulated about the recipe temperature set-point. The temperatures of the other thermocouples are regulated about the sum of the temperature set-point and the corresponding offset. For example, suppose the temperature set-point is given in the recipe as 700 C, and the front offset is given as -20 C. Then the center temperature is regulated about 700 C and the front temperature is regulated about 680 C. Use of the offsets has the effect of creating four separate temperature set-points. However, even with the additional degrees of freedom, the authority to control the entire susceptor temperature profile is limited. The profile can be set only roughly at points other than at the thermocouple locations. Offsets are currently set via trial-and-error and heuristic methods.

In the inlet flange currently installed in the Epsilon-1 at Northrop Grumman, there is a set of three gas injector slits with adjustable widths. These are used for adjusting the flow profile at the inlet to the process chamber. We note that the manual adjustment of slit widths is difficult, and the widths can be measured only approximately. In the future, this equipment will be replaced by a set of five injector port orifices with adjustable diameters. The new gas supply equipment will allow for tighter control and more degrees of freedom in determining the inlet flow profile. Either way, however, the authority to control the flow characteristics is once again limited. The manner in which the size of gas injector openings affect the flow profile is known only roughly. The size of gas injector openings are currently determined via trial-and-error and heuristic methods.

Wafer rotation is used to smooth non-uniform heating and other effects. It is typically set at 35 RPM for most, if not all, production runs.

3.5 Operating Structure

An overview of the general operating structure of the Epsilon-1 reactor, from the viewpoint of how recipe inputs and equipment settings affect reactor operation, is presented in Figure 3. Note that the internal details of individual blocks are not included here. They will be discussed whenever relevant later in this report. Of particular interest is the process chamber block, which contains physical and chemical mechanisms for film growth.

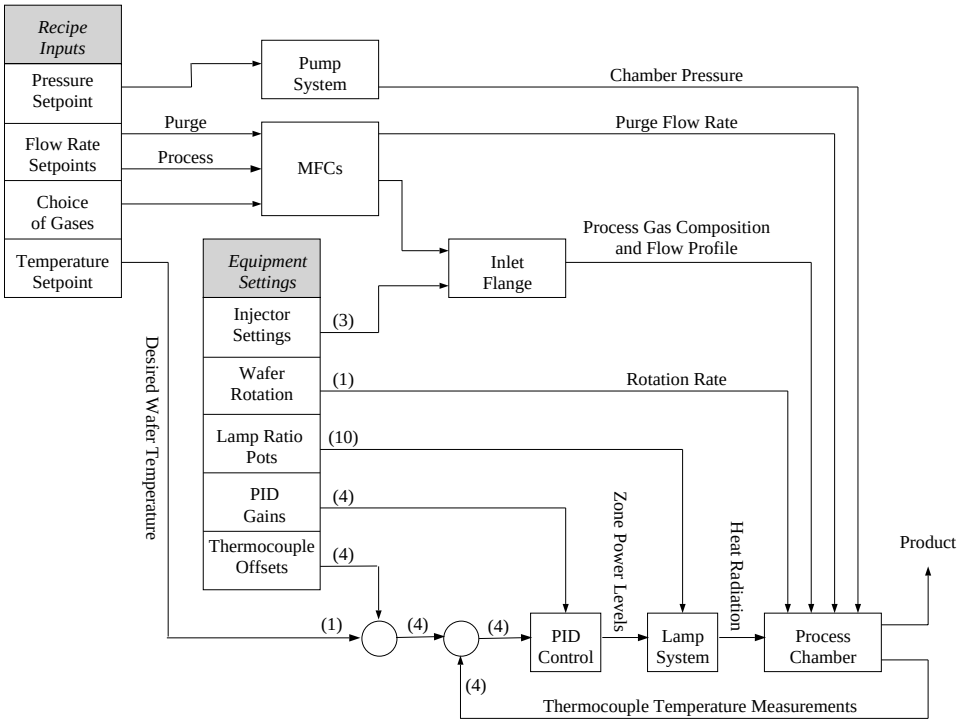

Figure 3: Overview of general operating structure of ASM Epsilon-1 reactor, from the viewpoint of how recipe inputs and equipment settings affect reactor operation. Numbers in parentheses refer to the number of distinct signals in the associated path.

4 Process-Equipment Model

This section motivates and describes the process-equipment model that we developed to predict process behavior (transient and steady-state) and product characteristics. We loosely describe the model as comprehensive because it accounts for a wide range of physical and chemical mechanisms, reactor geometry, material properties, and the effects of process conditions (pressure, temperature, flow rates, and gas composition) and equipment settings (injector sizes, thermocouple offsets). This does not imply that the model represents a complete description of process-equipment dynamics (if such a model is actually possible). Rather, we made choices so that the importance of a particular effect would be reflected in the model fidelity.

4.1 Motivation: Uniformity Case Study

The ultimate purpose of the process-equipment model is to predict the steady state deposition rate with emphasis on the spatial distribution of film thickness. It is crucial, then, to identify those phenomena that are important to determining growth rate, and include the effects of those phenomena in the model. It is also necessary to identify and include relevant features of the reactor geometry and operation, and to incorporate sufficient spatial resolution and dimensionality.

For thermally activated thin film growth, it is usually assumed or implied in the literature that achieving deposition uniformity is tantamount to achieving temperature uniformity across the wafer surface. Optimization and control strategies are then designed to achieve the temperature uniformity objective via manipulation of lamp power settings, so that deposition uniformity is achieved via automatic lamp control. Examples of such studies can be found in [3, 4, 8, 25, 26, 27]. Sometimes the assumption is justified by stating that wafer rotation will average out all other factors.

However, the assumption of equivalence between temperature uniformity and deposition uniformity does not necessarily hold, even for thermally driven processes and processes in which the wafer is rotating. For example, consider the experience of Northrop Grumman with deposition of epi-Si or Si-Ge in the thermally driven regime (approximately 600–800 degrees C) in the Epsilon-1 reactor. The process engineer achieves thickness variations of less than 1.5%

(considered acceptable uniformity) for a non-rotating wafer by setting thermocouple offsets at -25, -60, and -35 for front, rear, and side, respectively [23]. These values were determined via trial-and-error growth experiments. If growth rate were affected only by temperature and no other factors, then the 1.5% thickness variation that is achieved with those offsets would correspond to a 0.075% temperature variation across the wafer surface, or roughly 0.5 degrees C. However, for a recipe temperature set-point of 700 C, the corresponding thermocouple set-points are center at 700 C, front at 675 C, rear at 640 C, and side at 665 C, for a maximum deviation of 8.5%, as illustrated in Figure 4. Thus, the non-uniformity imposed by the offsets appears to be significantly greater than that indicated by actual growth rates.

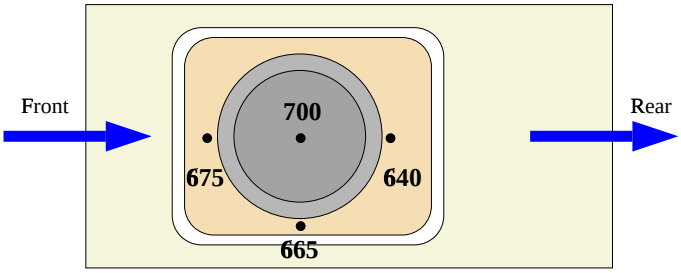

Figure 4: An example of how thermocouple offsets (front -25 C, rear -60 C, side -35 C) influence the temperature set-points around which the four thermocouples are regulated by PID controllers.

The set-up of the reactor apparatus may partially explain the smaller variation in actual growth rates. Recall that the front, rear, and side thermocouples are located in the ring surrounding the susceptor, rather than in the susceptor itself. Furthermore, the 6 inch diameter wafer is resting on quartz pins at the center of the 8.85 inch diameter susceptor. Therefore, it is reasonable to assume that the temperature variation across the wafer surface will be less than the variation across the entire susceptor. However, by similar reasoning, it is also intuitive that this could not entirely account for the thickness uniformity. For example, the front, rear, and side thermocouples are all the same distance from the center. But the offsets are not equal. The apparatus symmetry is not mirrored by the temperature set-points. Some other phenomena must be playing a role.

A quantifiable relationship between the offsets and the actual temperature field on the wafer surface is unknown. This is because there exists no reliable method for measuring temperature on the wafer surface. Poly–silicon growth rates are often used as a sensitive thermometer. While this method may be useful for measuring aggregate temperature, we argue here that it is flawed for measuring a temperature distribution across a surface, unless one can guarantee that other conditions across the surface (e.g., reactant concentrations) are perfectly uniform. The other alternative is to use an instrumented wafer, i.e., a wafer with attached thermocouples. However, ASM and Northrop Grumman consider measurements taken using the instrumented wafer to be unreliable, especially while operating at process conditions for growth [18, 23]. Nevertheless, we report that experiments using an instrumented wafer indicate maximum temperature variations of 5 degrees C or 0.7% [23]. This non-uniformity is less than that predicted by considering just the offsets and more than that found by measuring growth rates. In that respect, it appears to fall in the correct range.

Finally, we note that wafer rotation reduces the growth rate variation from 1.5% to less than 1% and temperature variations as recorded by the instrumented wafer from 5 C to 1 C. Therefore, we may conclude that wafer rotation does have the intended flattening effect, but does not compensate entirely for temperature non-uniformity.

We have demonstrated anecdotally that thickness and growth rate uniformity in the thermally activated regime is achieved by setting three thermocouple offsets so that the temperature distribution across the susceptor is intentionally non-uniform. The actual relationships among offsets, temperature, and growth rate, and the other factors that affect them, are left to be determined.

4.2 Process–Equipment State

It has become apparent that spatial uniformity of deposition rate and film thickness is influenced by several variables, not limited to wafer temperature, even for thermally driven processes. These variables are included in what we refer to as the *process-equipment state*, which is the time-varying spatial distribution of flow velocity, temperature, and species concentrations throughout relevant portions of the reactor. The time evolution and steady behavior of the process-equipment state is determined by the physical and chemical mechanisms of the CVD process, reactor geome-

try, material properties, recipe inputs, and equipment settings. The components of the process-equipment state interact with each other, the recipe inputs, and the equipment settings in a complex manner.

The process-equipment state is manifested in certain macroscopic phenomena that we believe have a significant influence on deposition uniformity. This is mainly due to the fact that they contribute to non-uniformity of reactant concentration profiles at or near the wafer surface. We wish to study these phenomena using the process-equipment model. Here we describe some of the important effects that we focused on in the modeling effort.

- **Reactant depletion:** As precursor gases flow across the wafer surface, reactants are deposited, causing a gradual downstream reduction in their gas phase concentration. Thus, downstream portions of the wafer may be subject to lower concentrations of impinging reactants, and hence the growth rate may be lower there. The magnitude of the depletion effect varies depending upon process conditions. The degree to which wafer rotation compensates for reactant depletion is not accurately known.

- **Nonuniform gas heating and gas phase reactions:** Based on experimental data, gas phase reactions appear to be important in CVD processes, except for those under very low pressure (see [14] pp. 134). For example, at atmospheric pressure, growth rate of silicon from silane is strongly influenced by dissociative deposition of intermediate species formed in the gas phase. Furthermore, gas phase reaction rates can be strongly dependent on temperature. Typically, the gases heat up as they pass over the susceptor and wafer in the process chamber. This may cause a gradual downstream increase in gas phase reaction rates. Thus, downstream portions of the wafer may be subject to higher concentrations of impinging reactants. The overall effect depends on the gas composition and process conditions.

- **Thermal diffusion of species:** The gas species in an initially homogeneous gas mixture will separate under the influence of a temperature gradient (see [14] pp. 110). Large, heavy molecules (e.g., silane) diffuse toward colder regions, whereas small, light molecules (e.g., hydrogen) diffuse toward hotter regions. Usually, the effect is small compared with ordinary concentration driven diffusion. However, due to the large thermal gradients in the cold-wall Epsilon-1 (e.g., 300 C difference between wafer and walls), thermal diffusion may have a significant effect. Thus, reactant concentration may be higher where the gas is cooler, e.g., upstream or in the lower section of the chamber. Reduction in growth rate by 20% to 30% caused by thermal diffusion has been observed in RTCVD chambers (see [14] pp. 164). Thermal diffusion is sometimes referred to as the Soret effect.

- **Flow patterns:** Previous calculations in [21] indicate a Reynolds number of approximately 27 for gas flow in the Epsilon-1. Thus, the flow is laminar, except possibly in and very close to the injector nozzles. Nevertheless, the flow may have some interesting characteristics that have an impact on deposition uniformity. Recirculation cells due to buoyancy effects are believed to occur in virtually all rapid thermal CVD (RTCVD) chambers due to the large thermal gradients present (see [1] pp. 339). Furthermore, three types of natural convection rolls are typically observed in horizontal CVD chambers: steady longitudinal, unsteady transversal, and steady transversal at the leading edge of the heated susceptor (see [14] pp. 162).

For each of the above effects, the relationship between it, the process-equipment state, recipe inputs, equipment settings, and thickness uniformity is not well understood. Moreover, it is not well understood how to compensate for non-uniformity in species concentrations caused by these effects. The setting of gas injector opening sizes and thermocouple offsets to minimize these effects and to produce uniform thickness is done iteratively, usually requiring approximately five test recipes. This modeling effort is a first step toward understanding these relationships and developing a model-based systematic compensation method.

4.3 Modeling Approach

The initial models presented in [21] considered the process-equipment state to be completely determined by a 1-dimensional (radial) wafer temperature profile. Growth rate was related to wafer temperature by a single nonlinear Arrhenius law. As stated earlier, this approach appears often in the literature (motivated by temperature control problems), but is inadequate for our purposes here.

Models incorporating more complete descriptions of transport phenomena, chemical mechanisms, couplings, 2-dimensional or 3-dimensional spatial effects, and non-symmetric geometries have been appearing recently in the literature. Authors have approached the modeling problem based on their specific objectives, process, and equipment, resulting in models with varying levels of detail and breadth of scope.

In [17] a dynamic simulator is presented which predicts the time–dependent behavior of equipment, process, sensors, and control systems for RTCVD of poly-Si from silane. This simulator is comprehensive in the respect that it provides the capability to predict aggregate values for deposition rate, film thickness, temperature, and gas flow, as well as cycle time, consumables volume, and reactant utilization. However, prediction of deposition uniformity requires high spatial resolution, rather than aggregate quantities, so their approach is not suitable here.

Axisymmetric cylindrical vertically oriented reactors are considered in [2, 7]. They incorporate coupled effects of 2-dimensional gas flow, mass transport, and heat transfer effects. In addition, [7] includes thermal diffusion and the effect of susceptor rotation on the gas flow. These models consider a relatively broad scope of effects for reactors with simple geometries that can be analyzed and simulated at high resolution in two spatial dimensions. They do not include models of chemical mechanisms for growth.

Models for reactors with non-symmetric geometries that require consideration of 3-dimensional effects are scarce. This is mainly due to the significant additional complexity of equations, boundary conditions, and solution techniques, along with burdensome computational demands. One strategy is to restrict the effort to one particular effect of interest. Two such models for commercial RTCVD chambers, that are limited to heat transfer only, including complicated surface-to-surface radiation, are presented in [11, 15].

Another strategy is to use commercially available general purpose computational fluid dynamics (CFD) codes and software packages. These packages provide the necessary tools for modeling of transport phenomena coupled with some chemical mechanisms, including efficient numerical integration schemes and 3-dimensional grid generation for irregular geometries. The CFD approach provides a comprehensive and general process-equipment state description.

However, there are drawbacks to using general purpose CFD packages. There is an interface layer in the software that separates the user from the underlying computer code and variables. This is advantageous for setting up problems but makes it difficult to use CFD code in control loops or other specialized applications. The general purpose nature of the software results in some built-in limitations to the level of accuracy and detail that can be achieved in modeling specific aspects of a particular piece of equipment. It is unclear how to channel computational resources to areas in accordance with their importance, or to deal efficiently with phenomena that occur at vastly different spatial and temporal scales. CVD applications present special challenges, including modeling for transport of mass and momentum in a multicomponent gas mixture, heat radiation with spectral dependence, and surface chemistry.

Some of the above problems related to CVD applications were addressed by the ESPRIT ACCESS-CVD project funded by the European Commission to develop and implement a CFD code specifically designed for use in modeling CVD processes. The project resulted in a commercial code, PHOENICS-CVD, which makes it practical to include many of the important effects associated with CVD processes. It consists of coupled dynamic sub-models for fluid flow, heat transfer, and multicomponent species transport in the gas phase, integrated with a model for conjugate heat transfer among lamps and other solid surfaces, databases and models for gas phase and surface chemistry for a large number of reactions, and databases and models for determining the time-varying, parameter dependent transport, thermodynamic, and optical properties of the involved materials.

The PHOENICS-CVD software was used to model a variety of CVD reactors in a semiconductor development line for 0.3 μm CMOS devices as presented in [29]. Most importantly for our purposes, the authors demonstrated the capability of PHOENICS-CVD as a tool for investigating uniformity issues in reactors with non-symmetric geometries.

Given project objectives, and in light of the complicated geometry and operation of the Epsilon-1 reactor, we implemented Epsilon-1 reactor simulations using PHOENICS-CVD. Figure 5 shows a general overview of the modeling framework. For a detailed exposition on the various aspects of this type of model see [14]. The idea is to produce a model that predicts the behavior of the process chamber block shown previously in Figure 3. Process recipe inputs and equipment settings enter the model via material parameters, boundary conditions on transport variables, and geometric construction of the solution grid. We note that even using the powerful PHOENICS-CVD tool, high-fidelity models that include most or all of the desired features previously described is an immensely time consuming undertaking. For this reason, various simplifications are still employed, which are described in the sequel as they are encountered.

4.4 Reactor Geometry and Finite Volume Mesh

The non-symmetric geometry of the Epsilon-1 necessitates genuine 3-dimensional modeling of transport phenomena in the process chamber. We adopt a Cartesian (x-y-z) coordinate system, since the lenticular chamber can be modeled roughly as long thin box with polygonal or curved sides.

We refer to the direction of flow from front to rear as the z direction, the bottom to top direction (perpendicular to the wafer) as the y direction, and the left side to right side direction (looking in through front) as the x direction. These

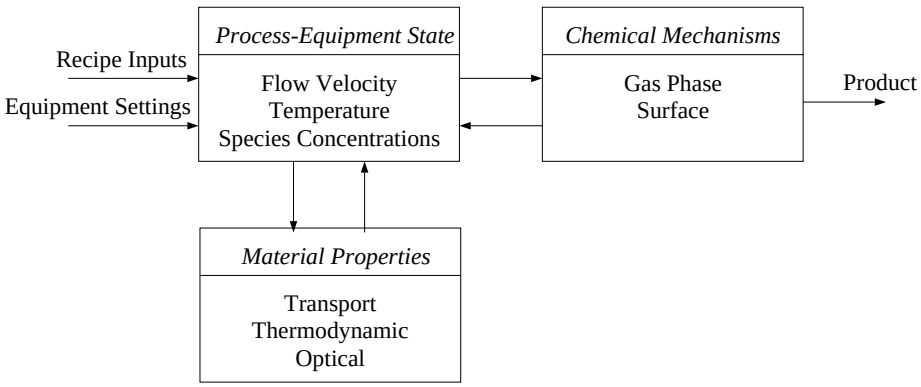

Figure 5: Overview of modeling framework. Process-equipment state components (gas flow, heat transfer, species transport) are coupled to each other, material properties, and chemical mechanisms.

coordinates are natural and convenient for chamber modeling but not for modeling the cylindrical wafer and susceptor, whose geometries must then be approximated.

PHOENICS uses a finite-volume mesh as the discretization of the spatial domain. Figure 6 shows a view of the overall mesh we developed for modeling the Epsilon-1 process chamber. The mesh is body-fitted and has dimensions of 25 by 27 by 52 volume elements in the x, y, and z directions, respectively.

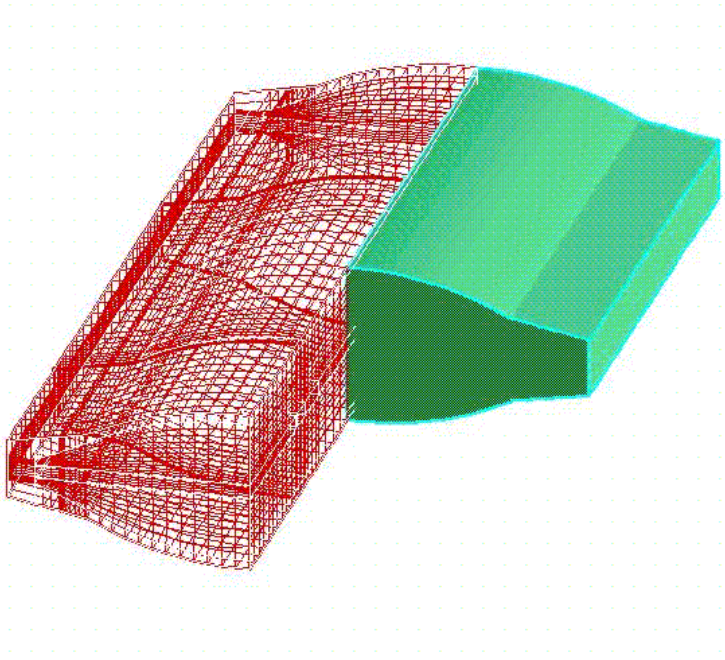

Figure 6: Overall body-fitted $25 \times 27 \times 52$ finite volume mesh for modeling ASM Epsilon-1 lenticular chamber. Solid cut-away figure at right is a viewing aide to show the full geometry of the chamber, but not part of the mesh. Inlet side faces viewer.

The Epsilon-1 apparatus set-up and gas flows are not symmetric in the y- and z-directions. Although the exterior geometry appears to be y-symmetric, there are significant differences between upper and lower chamber sections. The chamber does have x-symmetry, with the center y-z plane serving as a symmetry plane about which the geometry and values for all variables are mirrored exactly. The shaded portion on the right side of Figure 6 is not part of the actual mesh, but rather a viewing aide to show a portion of the overall chamber geometry. Only the left half of the chamber is modeled.

Figure 7 shows a top view of the *x*-*z* mid-plane level with the wafer surface. The surface geometry of the wafer, susceptor, and ring have been approximated by rectangular sections. It is possible to approximate the curved surfaces more accurately, either with additional rectangular volume elements arranged appropriately, or with irregularly shaped volume elements. However, irregularly shaped volume elements caused computational difficulties, and construction of the disk shape from regular elements required a large number of additional mesh elements in areas that were not of particular interest. These drawbacks offset any advantages gained from improving the geometrical accuracy of the wafer.

Figure 8 shows a side view of the center *y*-*z* plane. The upper and lower chamber sections can be identified, respectively, above and below the wafer. Gases can flow and species can diffuse between the upper and lower chamber sections through thin gaps between the quartz shelf and the ring, and between the ring and susceptor. We model only the shelf-ring gap since it is significantly wider than the ring-susceptor gap, and assume that it accounts for all interaction between upper and lower sections.

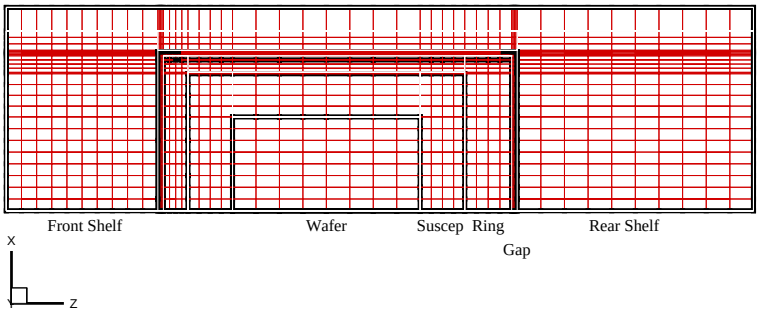

Figure 7: Top view of finite volume mesh at x-z mid-plane level with wafer surface.

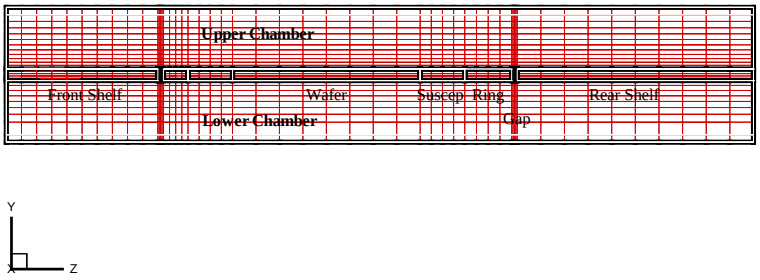

Figure 8: Side view of finite volume mesh at y-z mid-plane which serves as a symmetry plane.

In addition to the chamber model, we have also developed a simplified 3-dimensional finite-volume mesh for the inlet flange. This mesh uses three thin gaps in a solid surface to model the three injector slits. The gas mixture flows vertically downward from an inlet opening through the slits until it reaches the bottom surface of the inlet flange, at which point it is forced to make a perpendicular change of direction toward the chamber entrance. The idea is to simulate the effects that the injector slits and the injector flange geometry has on the flow. For example, we are interested in seeing how the forced change of direction creates possible swirling effects, and how varying injector slit widths affects the flow profile as gases enter and flow through the chamber. This model is separate from the chamber model, which assumes a uniform flow profile at the inlet to the chamber.

4.5 Transport Phenomena

The process-equipment state is determined by the transport of mass, momentum, and heat energy in the process and purge gases, and heat energy in and among the solids that comprise the chamber walls, shelves, ring, susceptor, and

wafer. The various effects are coupled through transport equations, state dependent material parameters, and boundary conditions. We provide here a brief overview of the main assumptions and equations used in the PHOENICS-CVD transport models. Further details can be found in [13, 14].

4.5.1 Assumptions

The basic assumptions regarding the gas mixture are that it behaves as a continuum, is an ideal gas, and is transparent to infrared heat radiation. In addition, the flow is assumed to be laminar and the effects of viscous heating and pressure variations on the gas temperature is neglected. These assumptions are widely applicable to CVD systems and in particular are not limiting for modeling the Epsilon-1.

We also made assumptions regarding boundary conditions that are specific to modeling the Epsilon-1. The flow profile at the entrance to the chamber is assumed to be a uniform flow velocity in the direction normal to the entrance. All solids in the chamber are considered isothermal, i.e., constant temperature within each individual piece of apparatus and throughout the entire wafer. Chamber walls are assumed to be no-slip and stationary, even though in reality there are moving parts in the process chamber. We assume that the top surface of the wafer is the only surface on which chemical reactions occur. These assumptions can limit the scope of the predictive capability of the model. However, we believe that they do not seriously degrade model fidelity regarding prediction of steady-state phenomena, so long as they are accounted for in any investigation of the factors that influence uniformity. The assumptions are discussed further in Section 4.7.

4.5.2 Gas Phase Transport

We now give the basic transport equations for an N-component reacting gas mixture with K gas phase reactions. Gas flow in the reactor is described by the familiar conservation equations for mass and momentum, i.e., the continuity equation

$$\frac{\partial \rho}{\partial t} = \nabla \cdot (\rho \underline{v}) \tag{1}$$

and the Navier-Stokes equation

$$\underbrace{\frac{\partial (\rho \underline{v})}{\partial t}}_{\text{transient}} = \underbrace{-\nabla \cdot (\rho \underline{v}\underline{v})}_{\text{inertial}} + \underbrace{\nabla \cdot \underline{\underline{\tau}}}_{\text{viscous}} - \underbrace{\nabla P}_{\text{pressure}} + \underbrace{\rho \underline{g}}_{\text{gravity}} \tag{2}$$

where ρ is the gas density, $\underline{v}$ is the gas velocity, P is the pressure, and $\underline{g}$ is gravity. The viscous stress tensor $\underline{\underline{\tau}}$ for a Newtonian fluid such as the gas mixture in a CVD reactor takes the form

$$\underline{\underline{\tau}} = \mu \left(\nabla \underline{v} + (\nabla \underline{v})^{\mathrm{T}} \right) - \frac{2}{3} \mu (\nabla \cdot \underline{v}) \cdot \underline{\underline{\mathbb{1}}} \tag{3}$$

where μ is the dynamic viscosity of the gas. For CVD applications, the density ρ and viscosity μ are strongly dependent on the temperature, pressure, and mixture composition. For this reason, the gas flow equations are strongly coupled to the equations for transport of heat energy and species concentrations. In particular, temperature and concentration gradients cause variations in gas mixture density which are manifested in buoyancy effects.

Transport of heat energy in the reactor is described by the familiar heat equation, with additional terms to account for effects that occur in chemically reacting multicomponent gases. In particular, heat is generated and consumed by the inter-diffusion of different species and by the various gas phase chemical reactions. Also, heat can flow due to the presence of a concentration gradient, which is referred to as the Dufour effect. The conservation equation for gas temperature is given by

$$\begin{aligned} \underbrace{c_p \frac{\partial (\rho T_g)}{\partial t}}_{\text{transient}} = & \underbrace{\nabla \cdot (k_c \nabla T_g)}_{\text{conduction}} + \underbrace{c_p \nabla \cdot (\rho \underline{v} T_g)}_{\text{convection}} + \underbrace{\nabla \cdot \left(R_g T_g \sum_{i=1}^{N} \frac{D_i^T}{m_i} \nabla (\ln f_i) \right)}_{\text{Dufour}} + \\ & \underbrace{\sum_{i=1}^{N} \frac{H_i}{m_i} \nabla \cdot \underline{j}_i}_{\text{inter-diffusion}} - \underbrace{\sum_{i=1}^{N} \sum_{k=1}^{K} H_i \nu_{ik} \left(R_k^g - R_{-k}^g \right)}_{\text{reactions}} \end{aligned} \tag{4}$$

where c_p is the specific heat capacity per unit mass of the gas, T_g is the gas temperature, k_c is the gas thermal conductivity, and R_g is the universal gas constant. Associated with the i-th gas species is the mole fraction f_i, molar mass m_i, thermal diffusion coefficient D_i^T, molar enthalpy H_i, and total diffusive mass flux $\underline{j}_i$. The stoichiometric coefficient of the i-th species in the k-th gas phase reaction is denoted ν_{ik} with forward reaction rate R_k^g and reverse reaction rate R_{-k}^g.

PHOENICS-CVD ignores the Dufour effect since it has been found to be very small in CVD systems. The density, viscosity, thermal conductivity, specific heat capacity, and thermal diffusion coefficient are dependent on temperature and gas mixture composition. For this reason, the heat transfer equation is strongly coupled to the gas flow and species concentration equations.

Gas species transport in the reactor is described by a familiar diffusion-convection equation with an additional source term to account for the creation and destruction of species due to K reversible chemical reactions. The balance equation for the concentration of the i-th gas species is given by

$$\underbrace{\frac{\partial(\rho\,\omega_i)}{\partial t}}_{\text{transient}} = \underbrace{-\nabla\cdot(\rho\,\underline{v}\,\omega_i)}_{\text{convection}} - \underbrace{\nabla\cdot\underline{j}_i}_{\text{diffusion}} + \underbrace{m_i\sum_{k=1}^{K}\nu_{ik}\left(R_k^g - R_{-k}^g\right)}_{\text{reactions}}. \tag{5}$$

In the above, the concentration of the i-th gas species is a dimensionless mass fraction

$$\omega_i = \frac{\rho_i}{\rho}.$$

There are $N-1$ independent species concentration equations of the form (5) since the mass fractions must sum to 1, i.e.,

$$\sum_{i=1}^{N}\omega_i = 1.$$

The diffusive mass fluxes are defined by

$$\underline{j}_i = \rho\,\omega_i\,(\underline{v}_i - \underline{v})$$

with respect to the mass averaged velocity

$$\underline{v} = \sum_{i=1}^{N}\omega_i\underline{v}_i$$

and satisfy

$$\sum_{i=1}^{N}\underline{j}_i = 0$$

again leaving $N-1$ independent variables.

Gas species diffusion is caused by concentration gradients, which we refer to as ordinary diffusion, and by temperature gradients, which we refer to as thermal diffusion, or the Soret effect. It is expressed as the sum of these two components

$$\underline{j}_i = \underline{j}_i^{\mathrm{C}} + \underline{j}_i^{\mathrm{T}}$$

where $\underline{j}_i^{\mathrm{C}}$ and $\underline{j}_i^{\mathrm{T}}$ denote the concentration driven and thermally driven diffusive fluxes, respectively. The ordinary diffusive mass fluxes can be computed via Fick's law, the Wilke approximation, or the full Stefan-Maxwell equations, depending upon the properties of the gas mixture, the desired degree of fidelity, and the available computational resources. The Stefan-Maxwell formulation is given by

$$\nabla\omega_i + \omega_i\nabla(\ln m) = \frac{m}{\rho}\sum_{j=1}^{N}\frac{1}{m_j D_{ij}}\left(\omega_i\,\underline{j}_j^{C} - \omega_j\,\underline{j}_i^{\mathrm{C}}\right) \tag{6}$$

with m the average mole mass of the mixture. The diffusive mass fluxes due to thermal diffusion are given by

$$\underline{j}_i^{\mathrm{T}} = -D_i^T\nabla(\ln T_g) \tag{7}$$

where the thermal diffusion coefficient D_i^T for each species is a function of temperature and gas mixture composition. In general $D_i^T > 0$ for large, heavy molecules and $D_i^T < 0$ for small, light molecules, resulting in the observed separation of species due to thermal gradients.

The last term in the species concentration equation (5) represents the creation and destruction of the i-th species due to homogeneous gas phase reactions. The forward and reverse reaction rates are given by

$$R_k^g = k_g(P,T) \prod_{\text{reactants}} \left(\frac{P f_i}{R_g T} \right)^{|\nu_{ik}|} \tag{8}$$

$$R_{-k}^g = k_{-g}(P,T) \prod_{\text{products}} \left(\frac{P f_i}{R_g T} \right)^{|\nu_{ik}|} \tag{9}$$

where k_g and k_{-g} are the forward and reverse reaction rate constants, and P the total pressure.

4.5.3 Boundary Conditions

For each of the gas phase transport equations there is an associated set of boundary conditions, which prescribe the state (or associated flux) at the inlet, outlet, chamber walls, and chamber apparatus including susceptor and wafer. The boundary conditions for temperature and species concentrations are responsible for coupling the gas phase transport phenomena to heat transfer in the solids and wafer surface chemical reactions, respectively. We elaborate further below.

For each inlet boundary (process and purge), we prescribe the inflow velocity of the gas mixture normal to the inflow opening, and the mass fraction for each of the gaseous species (e.g., silane and hydrogen). The values are set according to the process recipe we wish to simulate. The temperature of the gas mixture at the inlet is set to room temperature. There is no species diffusion through the inlet. These conditions are given by

$$\underline{n} \cdot \underline{v} = v_{\text{in}}\,, \quad \underline{n} \times \underline{v} = 0\,, \quad T = T_{\text{room}}\,, \quad \omega_i = \omega_{i,\text{in}}\,, \quad \underline{n} \cdot \underline{j}_i = 0 \tag{10}$$

where n is the unit vector normal to the inlet opening.

For the outlet boundary, we impose zero gradient conditions for all variables. These conditions are given by

$$\underline{n} \cdot (\nabla (\rho \underline{v})) = 0\,, \quad \underline{n} \times \underline{v} = 0\,, \quad \underline{n} \cdot (k_c \nabla T_g) = 0\,, \quad \underline{n} \cdot \underline{j}_i = 0 \tag{11}$$

where n is the unit vector normal to the outlet opening.

Boundary conditions at the solid-gas interfaces can be more complicated, mainly due to chemically reacting surfaces and heat transfer in the solids. First we consider non-reacting surfaces, e.g., chamber walls, quartz shelves, ring, and susceptor. At these surfaces, the no-slip and impermeability conditions apply, i.e., flow velocities are set to zero. Also, the total mass flux normal to each non-reacting surface must be zero for each of the species. Note, however, that due to thermal diffusion, the concentration gradients normal to the surface will generally not be zero. These conditions are given by

$$\underline{v} = 0\,, \quad \underline{n} \cdot \underline{j}_i = 0 \tag{12}$$

where n is the unit vector normal to the non-reacting surface.

For a reacting surface, which in our case refers only to the top side of the wafer, there is a net mass production rate for each gaseous species. The velocity component normal to the surface is proportional to this rate, while the tangential component is zero. Furthermore, the total mass flux normal to the reacting surface is set equal to the production rate. These conditions for a process with L surface reactions are given by

$$\underline{n} \cdot \underline{v} = \frac{1}{\rho} \sum_{i=1}^{N} m_i \sum_{l=1}^{L} \sigma_{il} R_l^s\,, \quad \underline{n} \times \underline{v} = 0\,, \quad \underline{n} \cdot \left(\rho \omega_i \underline{v} + \underline{j}_i \right) = m_i \sum_{l=1}^{L} \sigma_{il} R_l^s \tag{13}$$

where n is the unit vector normal to the reacting surface, σ_{il} is the stoichiometric coefficient for the i-th gas species in the l-th surface reaction, and R_l^s is the reaction rate for the l-th surface reaction. The surface reaction rate is equal to the product of the collision rate of molecules with the wafer surface and the reaction probability, called the reactive sticking coefficient (RSC).

Thermal boundary conditions at the solid-gas interfaces can be complex due to heat transfer within and among the various solids in the reactor. This includes the effects of conduction within the solids, convective losses to the gas phase, and radiative transfer among the various surfaces. Heat radiation supplied by the lamps is especially important.

PHOENICS-CVD provides the capability for modeling heat transfer in the solids and coupling these effects to the gas phase transport phenomena via boundary conditions. Surface-to-surface radiation is modeled using viewfactor

methods. However, due to the extremely complicated geometry of the Epsilon-1 lamp-house and reflector apparatus, and the very large number of solid surfaces with varying optical properties in the process chamber, we found the PHOENICS-CVD radiation modeling tool to be impractical for our purposes. This is discussed further in Section 4.7.

Instead of modeling heat transfer in the solids, we assumed that the wafer and susceptor were at a constant uniform temperature, and used anecdotal and experimental data from the manufacturer to estimate the temperature on other surfaces. The boundary conditions are given by

$$T_g = T_{\text{surf}}$$

for the case where the gas-solid interface is a isothermal surface and

$$\underline{n} \cdot \nabla T_g = 0$$

when there is an adiabatic surface.

Specific values for the boundary conditions were set according to the process recipes that we were simulating. Values are provided as simulations are described in Section 5.

4.5.4 Material Properties

Models for describing the dependence of material properties on the process-equipment state are presented in [13, 14] and included in the PHOENICS-CVD software. Furthermore, PHOENICS-CVD provides databases containing any necessary parameters for determining the transport, thermodynamic, and optical properties of most materials commonly used in CVD processes.

Transport properties of the gases include viscosity, thermal conductivity, and ordinary and thermal diffusion coefficients. Their dependence on temperature, pressure, and gas mixture composition is determined using the Lennard-Jones potential and kinetic theory. Lennard-Jones parameters for the individual gases are provided in a database. Properties of the gas mixture are calculated from the individual gas properties. For example, a semi-empirical relationship is employed for determining mixture viscosity.

Thermodynamic properties of the gases include specific heat capacity, standard heat of formation, and standard entropy. These properties are given as functions of temperature via polynomial approximations, with a different polynomial for each of three temperature ranges. Polynomial coefficients for individual gases are provided in a database. Again, properties of the gas mixture are calculated from the individual gas properties. For example, density is defined in terms of the mean molecular mass and specific heat is defined as the mass averaged value.

Optical properties of the solids include refractive indices and absorption coefficients. The temperature dependence of these properties in each of 60 spectral intervals is provided in a database. However, as stated earlier, we did not use the PHOENICS-CVD surface-to-surface radiation model, so the optical properties of the solids, e.g., quartz, do not play a role in our simulations.

4.6 Chemical Mechanisms for Growth

The relationship between silicon growth rate and wafer temperature was investigated via poly-Si growth experiments in [21]. There, it was shown that for a range of operating conditions, a simple Arrhenius law provides an accurate model for predicting growth rate as a function of wafer temperature. The model was given by

$$R_{\text{Si}} = k_0 \exp\left(\frac{-E_a}{R_g T_w}\right) X_{\text{SiH}_4} \tag{14}$$

where R_{Si} denotes silicon growth rate, k_0 denotes a pre-exponential constant, E_a denotes the activation energy for the surface reaction, R_g denotes the universal gas constant, T_w denotes the wafer temperature, and X_{SiH_4} denotes the mole fraction of silane in the gas mixture at the inlet. The Arrhenius law was adopted as the kinetics model, and parameters such as activation energy were calculated by fitting the experimental data to the model.

There are several assumptions and simplifications, both explicit and implicit, in the above Arrhenius model. It assumes that silicon growth is almost completely due to the heterogeneous decomposition of silane into silicon and hydrogen on the wafer surface. Thus, it models only a single surface reaction step. Furthermore, it is implicitly assumed that inlet conditions for silane mole fraction hold constant throughout the process chamber. This allows for a separation of the factor multiplying the exponential term into a mole fraction variable and a pre-exponential constant. The result is that growth rate is assumed to be dependent entirely on two process recipe inputs: wafer temperature

set-point and silane mole fraction at the inlet; and two process dependent physical-chemical parameters: activation energy and pre-exponential constant.

The above approach takes the view that surface reactions are dominant and gas phase reactions are negligible. However, it was demonstrated by Coltrin and co-workers [5] that as chamber pressure increases, gas phase reactions play a greater role. They showed that at atmospheric pressure, silicon growth may be almost completely due to reactive intermediaries formed in the gas phase.

Kleijn develops a model for gas phase and surface chemistry in [12] for temperatures and pressures in an intermediate range, near the conditions at which Northrop Grumman deposits silicon in the Epsilon-1. It is a relatively closed subsystem of the full kinetic model that was used by Coltrin and co-workers. The key reaction is the homogeneous decomposition of silane which leads to the formation of silylene (SiH_2), and hydrogen. Further reactions produce disilane (Si_2H_6), trisilane (Si_3H_8), and silylsylene (Si_2H_4). The five step gas phase reaction mechanism is given by

$$SiH_4 \overset{\leftarrow}{\rightarrow} SiH_2 + H_2 \tag{15}$$
$$Si_2H_6 \overset{\leftarrow}{\rightarrow} SiH_4 + SiH_2 \tag{16}$$
$$Si_3H_8 \overset{\leftarrow}{\rightarrow} Si_2H_6 + SiH_2 \tag{17}$$
$$Si_2H_4 \overset{\leftarrow}{\rightarrow} SiH_2 + SiH_2 \tag{18}$$
$$Si_2H_6 \overset{\leftarrow}{\rightarrow} Si_2H_4 + H_2 \tag{19}$$

each of which has an associated forward and reverse reaction rate constant, respectively, k_g and k_{-g}. For silicon growth at the wafer surface from silane and the reactive intermediaries, Kleijn uses a set of five surface reactions given by

$$SiH_4(g) \rightarrow Si(s) + 2H_2(g) \tag{20}$$
$$SiH_2(g) \rightarrow Si(s) + H_2(g) \tag{21}$$
$$Si_2H_6(g) \rightarrow 2Si(s) + 3H_2(g) \tag{22}$$
$$Si_3H_8(g) \rightarrow 3Si(s) + 4H_2(g) \tag{23}$$
$$Si_2H_4(g) \rightarrow 2Si(s) + 2H_2(g) \tag{24}$$

each of which has an associated RSC. We shall refer to the reaction schemes (15–19) together with (20–24) as the *Kleijn model* for poly-Si deposition.

The reaction rate constants and RSCs in the Kleijn model are derived from studies by various investigators. The gas phase forward and reverse reaction rate constants are, in general, temperature and pressure dependent, given by the expression

$$k_g = A P^{\kappa} \exp\left(\frac{-E_a}{R_g T_g}\right)$$

where parameters A and E_a were fitted to experimental data for temperatures from 300-1100 K and pressures from 10–100 Torr. Furthermore, each RSC is given by a different complicated function of wafer and gas temperature. Thus, the reaction scheme includes a complicated temperature dependence and is a function of a large number of physical-chemical parameters, e.g., multiple activation energies and multiple sticking coefficients.

PHOENICS-CVD provides the necessary tools to implement the Kleijn model, including a database of experimentally determined kinetics parameters. Thus, we used the Kleijn model to describe poly-Si chemical reaction kinetics in the Epsilon-1. In contrast to the initial simplified Arrhenius models, the chemistry model is coupled to the gas phase transport model, since gas phase reactions play an important role. Furthermore, no assumptions are made regarding the spatial distribution of temperature and reactant concentrations in the chamber.

4.7 Unmodeled Phenomena and Equipment

As stated earlier, even with powerful tools at our disposal, development of a comprehensive model that incorporates every relevant feature of the Epsilon-1 reactor is not practical. Here, we discuss some of the unmodeled features, phenomena, and processes that are relevant to growth in the Epsilon-1 but were not implemented in our models.

Si-Ge growth chemistry

Although reaction schemes including gas phase and surface reactions for growth of Si-Ge from silane and germane precursors have appeared recently in the literature, experimentally determined physical-chemical parameter values

for such schemes are proprietary information and in general not widely available. The authors are in contact with researchers at a government laboratory [19] regarding experiments to determine rate constants and sticking coefficients for Si-Ge growth.

Development of models for Si-Ge growth is particularly complicated due to the large number of phenomena involved and the manner in which the deposited film depends on the process-equipment state. For example, epitaxial Si-Ge layers are deposited using either dichlorosilane, silane, or disilane, along with germane. Deposition rate and germanium content have been observed to be dependent on the choice of precursor gas [10] and germane concentration [9]. Furthermore, both of these effects have been observed to be temperature dependent [6]. Thus, uniformity may be affected in different ways by non-uniform concentrations of different reactants at various temperatures.

Radiative heat transfer, lamp-house, and reflectors

Radiative heat transfer modeling is implemented in PHOENICS-CVD via viewfactor methods. This requires a discretization of the solid surfaces in the chamber into a large number of smaller surfaces that are considered isothermal and of constant optical properties. The predictive capability of the method depends on the number and size of the individual surfaces, which we refer to as the discretization resolution, as well as the accuracy of the chamber geometry implemented in the model.

Although the finite volume mesh used to model the chamber geometry is effective for capturing relevant gas phase transport phenomena, it neglects various features of the equipment which would have a significant effect on radiative heat transfer. Such features include apparatus containing wafer rotation machinery within the lower chamber section and the complicated lamp-house and reflector equipment. In the Epsilon-1, there are a variety of reflector designs, including both diffuse and specular, and some of a special parabolic shape. Also, certain parameters are known only roughly, such as the power supplied by the lamps, or equivalently the temperature of the filaments when they are turned on to 100% power. It is simply not practical to include the geometry and properties of these pieces of equipment in the finite volume reactor model.

Furthermore, in the Epsilon-1, there exist many transitions from one material to another, gaps between different pieces of the equipment, and a non-symmetric lenticular shape. This necessitates an extremely high discretization resolution for viewfactor modeling. For all of the above reasons, we believe that modeling of radiative heat transfer in the Epsilon-1 using the PHOENICS-CVD framework is too unwieldy and computationally expensive to be practical.

Currently, solid surfaces are modeled as isothermal, i.e., constant temperature within each individual piece of apparatus and throughout the entire wafer. Temperature values are set according to empirical data supplied by the manufacturer. In reality, temperature gradients exist within individual pieces of equipment, and the average steady-state temperature of any part of the reactor is known only roughly. However, it is not likely that implementation of a radiative heat transfer model using the PHOENICS-CVD framework would produce more accurate surface temperatures than manufacturer supplied empirical data.

We believe that a separate model restricted only to heat transfer within and among the solids in the Epsilon-1 is required. By limiting the scope of this additional model, and implementing it using a more flexible programming environment, it would be possible to reflect the relevant geometrical features at sufficiently high resolution to provide an accurate picture of the temperature distribution in the Epsilon-1 solids. Steady-state temperature values could then be used as boundary conditions in a refined process-equipment model. The heat transfer model developed in Phase I [21] serves as a starting point, but must be improved to include reflectors, chamber walls, quartz shelves, ring, and susceptor.

Wafer rotation

The actual mechanical rotation of the wafer is not accounted for in the models. CFD software routines for modeling of rotating objects in a flow environment are available, but require axisymmetry of the entire domain. Therefore, a separate effort would be required to investigate the effect of mechanical wafer rotation on the chamber flow immediately surrounding the wafer. The effect of wafer rotation on growth can be studied, partially, by performing averaging calculations on simulation results, i.e., averaging deposition rates around the wafer surface.

Rotation shaft purge

There is an additional purge gas inlet through the wafer rotation shaft. Purge gases injected through the rotation shaft enter the chamber directly underneath the center of the wafer. Recall that the wafer rests on small pins attached to the top of the susceptor. The purpose of the shaft purge is to prevent the source gases from flowing between the wafer and susceptor which could result in back-side deposition. Typically, the shaft purge is set to 3 slm H_2. This may have an effect on the chamber flow in the vicinity of the wafer. In addition, the presence of the rotation shaft would

affect the chamber flow in the lower chamber section. The rotation shaft and related apparatus are not included in the process-equipment model.

Deposition on chamber walls

The process-equipment model treats all surfaces other than the top surface of the wafer as non-reacting. However, deposition on other surfaces does occur in the Epsilon-1. As stated earlier, a build-up of such films is prevented by preceding the deposition step with a HCl etch clean. In Section 5.4, we slightly modify the process-equipment model so that the back-side of the susceptor becomes a reacting surface. This limited study could be expanded to study deposition on other chamber surfaces as well.

Chamber wall cooling

The quartz chamber and lamp-house are cooled by air flow. There is little data regarding characteristics of the air flow and convective losses from the outer wall of the chamber. These effects are not modeled. Instead, a constant temperature is set for each of the chamber walls.

5 Results and Applications

In this section we present results from poly-Si growth simulations using the Epsilon-1 process-equipment model. We use the simulation results to study various characteristics of the thin films and reactor operation that impact on manufacturing effectiveness. We show that the model can be used to predict growth rate and uniformity and to better understand the factors that influence these measures of performance. We also present simulation results that provide guidance toward improved setting of purge gas flow rates.

Because deposition times are typically much longer than initial transients in radiative heating and gas phase transport in the Epsilon-1, it is reasonable to assume that all growth occurs during steady-state operation. For this reason, all simulations described in this section predict steady-state values of growth rate and other variables.

5.1 Deposition Rate Prediction

We have performed poly-Si growth simulations using the Epsilon-1 process-equipment model to study the relationship between growth rate and the various process recipe inputs. Prediction of growth rate given process conditions is important for taking advantage of the flexibility of the Epsilon-1. The manufacturer provides some predictive guidance and data, but the process-equipment model can allow for prediction of growth rates "off-the-curve" and also provide a tool for performing multiple trial-and-error steps and for understanding the factors that influence growth rate and uniformity.

5.1.1 Wafer Temperature Sensitivity

In this section we investigate the relationship between silicon growth rate and wafer temperature in the Epsilon-1. This relationship had been studied previously in [21], where poly-Si growth rates were measured experimentally for a range of wafer temperatures (700, 725, 750 C) and silane flow rates (30, 50, 70 sccm) with pressure fixed at 20 Torr. It was shown that for the given range of operating conditions, a simple Arrhenius law provides an accurate model for predicting growth rate as a function of wafer temperature. Arrhenius model parameters such as activation energy were then calculated to fit the experimental data.

In contrast, the process-equipment model adopts the more complicated multi-step Kleijn model for silicon deposition. This growth model includes both gas phase and surface reactions, involves multiple reactive intermediaries, and is coupled to transport models. Because of the model's complicated nature, it is reasonable to expect difficulty in isolating the effect of wafer temperature on simulated growth rate. However, using reactor simulations, we show below that, like the experimentally determined growth rates, simulated growth rates can also be fitted to a simple Arrhenius law relating growth rate to wafer temperature. Furthermore, the single activation energy in the Arrhenius law fitted to simulated growth rates is nearly the same as that which was fitted to experimentally determined growth rates. Thus, there appears to be an underlying dominant chemical mechanism that obscures the effect of gas phase phenomena. We present the simulation results below.

The predictive capability of the process-equipment model was tested by simulating poly-Si growth using operating conditions for pressure, temperature, and flow rate that are duplicates of conditions used for experiments presented

in [21]. The boundary conditions used for the simulations are given in Table 1. The simulation results are presented in Table 2 together with corresponding experimental results from [21] .

In order to test the fit of simulated growth rates to an Arrhenius law, we plot the logarithm of growth rate as a function of inverse temperature, for each of the three flow rates used. The plots are shown, along with corresponding plots of experimental data, in Figure 9. Due to the linearity of the plot for simulation data, we can fit the simulation data to a simple Arrhenius law, where the slope of each plot is proportional to the activation energy. More importantly, the slopes of all plots are consistent over the range of flow rates, for both simulation and experimental data. This means that the activation energy for simulated growth is nearly identical to the activation energy measured for actual growth in the Epsilon-1. Calculated Arrhenius parameters for experimental and simulation data are presented in Table 3.

We note that the calculated activation energies fall within the range of published activation energies for deposition of silicon from silane for the given range of process conditions (see, e.g., [16]). In particular, they lie between the activation energy for silane adsorption (125 kJ/mol), which is associated with with temperatures above 700 C, and hydrogen desorption (192 kJ/mol), which is associated with temperatures below 700 C. Thus, it is likely that these are the dominant activating mechanisms for both actual and simulated growth.

However, other phenomena also play a role, resulting in the consistent upward shift from experimentally determined to simulated growth rates observed in the Arrhenius plots. By a consistent upward shift, we mean that the ratio of simulated to experimentally determined growth rates is a constant over the given range of operating conditions. We calculated this constant offset factor relating simulation and experimental data to have mean value 3.07 with standard deviation 0.11, as indicated in Table 2. Thus, the process-equipment model, using the Kleijn model for poly-Si growth chemistry, predicts growth rates that are roughly three times greater than actual growth rates. More importantly, this factor is constant over the selected range of temperatures and silane flow rates.

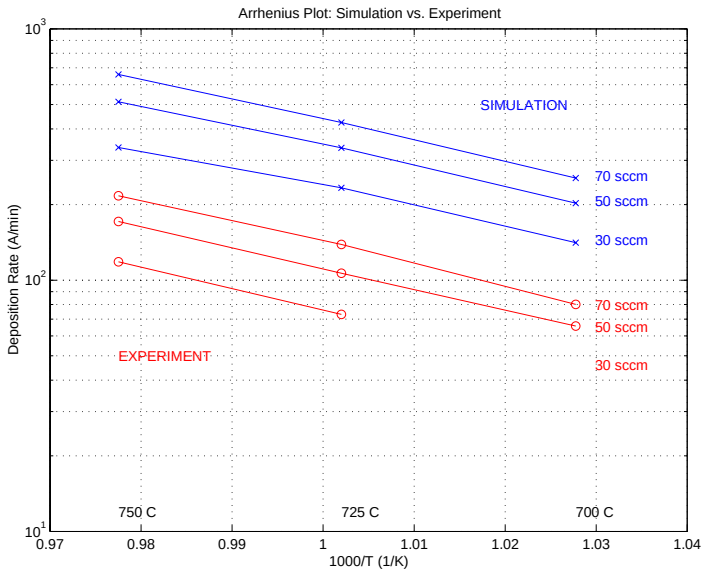

Figure 9: Plots illustrating Arrhenius relationship between poly-Si growth rate and wafer temperature in the Epsilon-1. Experimental and simulation data is taken for three silane flow rates (30, 50, and 70 sccm) and three temperatures (700, 725, 750 C) at 20 Torr. Simulated growth rates (top three plots) are a factor of 3.07 times greater than experimentally determined growth rates (bottom three plots) consistently over the given range of temperatures and flow rates.

We now offer some ideas toward a qualitative explanation of the presence of the offset factor. The Kleijn model is semi-empirical, i.e., it is based on phenomenological models and empirical data from growth experiments performed by various investigators. It is well known that rate constants and sticking coefficients for gas phase and surface reactions are difficult to measure, and reaction rates under nominally identical process conditions will vary among different reactors [23]. For example, Kleijn's study [12] used a cylindrical cold-wall chamber, which is very different from the lenticular hot-wall chamber in the Epsilon-1. Moreover, the process conditions used in the Kleijn study do not completely match those of our own. For example, Kleijn used pressures in the 1–10 Torr range (compared to our 20 Torr) and total flow rates on the order of 1 slm (compared to our $>$ 20 slm). The temperature ranges do coincide.

On the other hand, the consistency of the offset factor over a range of temperatures and silane flow rates indicates

Boundary Conditions Used In Epsilon-1 Reactor Simulations

Process Inlet Conditions
Carrier Gas H_2
Source Gas 2% SiH_4 in H_2

Condition	Values		
Flow Rate of Carrier (slm)	20	20	20
Flow Rate of Source (slm)	1.5	2.5	3.5
Flow Rate of Silane (sccm)	30	50	70
Mole Fraction of Silane ($\times 10^{-3}$)	1.40	2.22	2.98
Molar Mass of Silane (g/gmol)	32.12	32.12	32.12
Molar Mass of Gas Mixture (g/gmol)	2.06	2.08	2.11
Mass Fraction of Silane ($\times 10^{-2}$)	2.18	3.43	4.54
Density of Gas Mixture (kg/m$^3 \times 10^{-3}$)	2.25	2.28	2.30
Velocity of Gas Mixture (m/sec)	1.40	1.47	1.53
Temperature of Gas Mixture (C)	20	20	20

Purge Inlet Conditions
Purge Gas H_2

Condition	Value
Flow Rate of Purge Gas (slm)	7
Velocity of Purge Gas (m/sec)	0.45
Temperature of Purge Gas (C)	20

Solid-Gas Interface Conditions

Condition	Values		
Temperature of Wafer (C)	700	725	750
Temperature of Susceptor (C)	700	725	750
Temperature of Ring (C)	Conductive Solid		
Temperature of Front Quartz Shelf (C)	Conductive Solid		
Temperature of Rear Quartz Shelf (C)	Conductive Solid		
Temperature of Upper Chamber Wall (C)	400	425	450
Temperature of Lower Chamber Wall (C)	400	425	450

Table 1: Boundary conditions for process gas inlet, purge gas inlet, and solid surfaces used in simulations of poly-Si growth in the Epsilon-1 reactor.

Process-Equipment Model Predictive Capability
Growth Rate Temperature Dependence

Process Conditions	
Chamber Pressure	20 Torr
Carrier Gas	20 slm H_2
Source Gas	2% SiH_4 in H_2
Purge Gas	7 slm H_2

Growth Rate (A/min) Vs. Wafer Temperature and Silane Flow Rate

	Experiment			**Simulation**		
Wafer	Silane Flow Rate (sccm)			Silane Flow Rate (sccm)		
Temperature (C)	30	50	70	30	50	70
700		65.68	80.08	141.00	202.60	254.90
725	73.12	106.60	138.72	233.00	336.30	423.90
750	118.28	171.32	216.68	337.30	512.50	658.50

Ratio: Simulation / Experiment

Wafer	Silane Flow Rate (sccm)		
Temperature (C)	30	50	70
700		3.08	3.18
725	3.19	3.15	3.06
750	2.85	2.99	3.04

Mean	3.07
Standard Deviation	0.11

Note: Poly-silicon thickness for 750 C and 30 sccm was too small to be measured with available equipment.

Table 2: Results comparing poly-Si growth experiments with simulations. Growth rates are averaged over wafer surface.

Parameters of Arrhenius Relationship Fitted to Data
Experiment vs. Simulation

Assumed Relationship
$R_{Si} = C \exp\left(\frac{-E_a}{R_g T_w}\right)$

Process Conditions	
Chamber Pressure	20 Torr
Carrier Gas	20 slm H_2
Source Gas	2% SiH_4 in H_2
Purge Gas	7 slm H_2

Symbol	Description	Experiment			Simulation		
F_{SiH_4}	Silane Flow Rate (sccm)	30	50	70	30	50	70
E_a	Activation Energy (eV)	1.69	1.67	1.57	1.30	1.48	1.55
	Activation Energy (J/mol) ($\times 10^5$)	1.63	1.61	1.51	1.26	1.43	1.49
E_a/R_g	Ratio (K) ($\times 10^4$)	1.96	1.94	1.82	1.51	1.72	1.80
C	Pre-exponential Constant (A/min) ($\times 10^{10}$)	7.94	8.90	3.52	0.08	1.01	2.81

Table 3: Parameters calculated by fitting experimental and simulation data for poly-Si growth rates to an assumed Arrhenius relationship.

Growth Rate Pressure Dependence
Epsilon-1 Simulation

Process Conditions	
Carrier Gas	20 slm H_2
Source Gas	2% SiH_4 in H_2
Purge Gas	7 slm H_2

Simulated Growth Rate (A/min) Vs. Wafer Temperature and Silane Flow Rate

Chamber Pressure	**20 Torr**		**40 Torr**	
Wafer	Silane Flow Rate (sccm)		Silane Flow Rate (sccm)	
Temperature (C)	50	70	50	70
700	202.60	254.90	270.00	315.40
725	336.30	423.90	423.40	510.00
750	512.50	658.50	651.90	820.90

Ratio: 40 Torr / 20 Torr

Wafer	Silane Flow Rate (sccm)	
Temperature (C)	50	70
700	1.33	1.24
725	1.26	1.20
750	1.27	1.25

Mean	1.26
Standard Deviation	0.04

Table 4: Results from poly-Si growth simulations comparing growth rates at 20 Torr pressure with growth rates at 40 Torr pressure. Growth rates are averaged over wafer surface.

the likelihood that activation energies and sticking coefficients in the Kleijn model are close to those we would find by performing similar experiments in the Epsilon-1. It appears likely that the offset is due more to approximations and neglected effects in the process-equipment model. For example, discrepancies between actual and simulated gas phase flow, temperature, and species concentration distributions could alter the relative significance of each of the different reactive intermediaries. Thus, even if sticking coefficients for the five separate surface reactions are accurate, total growth rate would be shifted.

Beyond that, the coupling of gas phase reactions and transport phenomena with surface chemistry in the process-equipment model blurs any specific cause and effect relationships. It must also be emphasized that the model makes a number of approximations and assumptions whose cumulative effect is difficult to pinpoint. For example, the wafer geometry is approximated, so that the area of the wafer consuming reactants may not be modeled accurately.

By taking the offset factor of 3.07 into account, the model as it currently stands can be used to accurately predict silicon growth rate in the Epsilon-1 over a range of temperatures and silane flow rates typically used by Northrop Grumman. However, it would be preferable to improve the transport component of the model, and to conduct a more extensive experimental study, similar to Kleijn's, in which chemical kinetics parameters for growth in the Epsilon-1 are measured over a wide range of operating conditions.

5.1.2 Chamber Pressure Sensitivity

In this section we investigate the relationship between silicon growth rate and chamber pressure in the Epsilon-1. Actual growth rate is expected to increase as total pressure rises due to the increased number of molecular collisions on the wafer surface and the increased reaction rates of gas phase reactions. Simulation results presented below reflect this phenomenon.

We performed poly-Si growth simulations at a chamber pressure of 40 Torr using the same temperature and silane flow rate conditions as experiments and simulations performed at 20 Torr. However, due to time limitations, only two flow rates were used (50, 70 sccm). The simulation results for 20 Torr and 40 Torr are presented together in Table 4.

As before, we produced Arrhenius plots and calculated Arrhenius parameters in order to see how pressure affects

Parameters of Arrhenius Relationship Fitted to Simulation Data
Pressure Dependence

Assumed Relationship
$R_{Si} = C \exp\left(\frac{-E_a}{R_g T_w}\right)$

Process Conditions	
Carrier Gas	20 slm H_2
Source Gas	2% SiH_4 in H_2
Purge Gas	7 slm H_2

Symbol	Description	20 Torr		40 Torr	
F_{SiH_4}	Silane Flow Rate (sccm)	50	70	50	70
E_a	Activation Energy (eV)	1.48	1.55	1.52	1.68
	Activation Energy (J/mol) ($\times 10^5$)	1.43	1.49	1.47	1.62
E_a/R_g	Ratio (K) ($\times 10^4$)	1.72	1.80	1.77	1.95
C	Pre-exponential Constant (A/min) ($\times 10^{10}$)	1.01	2.81	1.98	14.77

Table 5: Parameters calculated by fitting simulation data for poly-Si growth rates to an assumed Arrhenius relationship.

growth rate. The results are presented in Figure 10 and Table 5. We see that growth rate increases by a factor of 1.26 as pressure increases from 20 Torr to 40 Torr. This offset factor is constant over the given range of operating conditions. This result is consistent with a study by Kleijn [12] in which growth rate increases as the logarithm (base 10) of pressure. Furthermore, activation energies for 40 Torr are slightly higher than those for 20 Torr but still within the expected range.

5.1.3 Flow Rate Sensitivity

We have studied the influence of silane flow rate on growth rate using the experimental and simulation data already presented. The recipe setting for silane flow rate directly affects two process variables concerning the gas mixture at the inlet, namely, silane mole fraction and overall gas velocity. As silane mole fraction increases, the contribution of gas phase reactions to the overall deposition process will be enhanced [12]. We now briefly discuss the relationship between flow velocity and deposition rate.

It is typically assumed that the gas stream can be divided into two regions. In the region away from the wafer surface, the gas stream is assumed to flow with relatively constant velocity, while in the region next to the wafer surface, there exists a stagnant boundary layer where the flow velocity is zero. In this model, mass transfer of the reactant species through the stagnant layer is dominated by a diffusion process. The mass flux Ψ impinging upon the wafer surface is proportional to the diffusion coefficient D and the difference between the reactant concentration in the full flow C_g and at the surface C_s, and inversely proportional to the thickness of the boundary layer δ, i.e.,

$$\Psi = \frac{D(C_g - C_s)}{\delta}. \tag{25}$$

Furthermore, the average boundary layer thickness δ is inversely proportional to the square root of the flow velocity V, i.e.,

$$\delta = C_1 V^{-1/2}.$$

The result is that the impinging flux of reactants Ψ is proportional to the square root of flow velocity, i.e.,

$$\Psi = C_2 V^{1/2}.$$

We express the relationship between deposition rate and flow velocity as a power law

$$R_{\mathrm{Si}} = C_3 V^{1/2}. \tag{26}$$

If the power law (26) provides an accurate model of the relationship between growth rate and flow velocity in the Epsilon-1, then the slope of a plot of the logarithm of growth rate versus the logarithm of flow velocity should

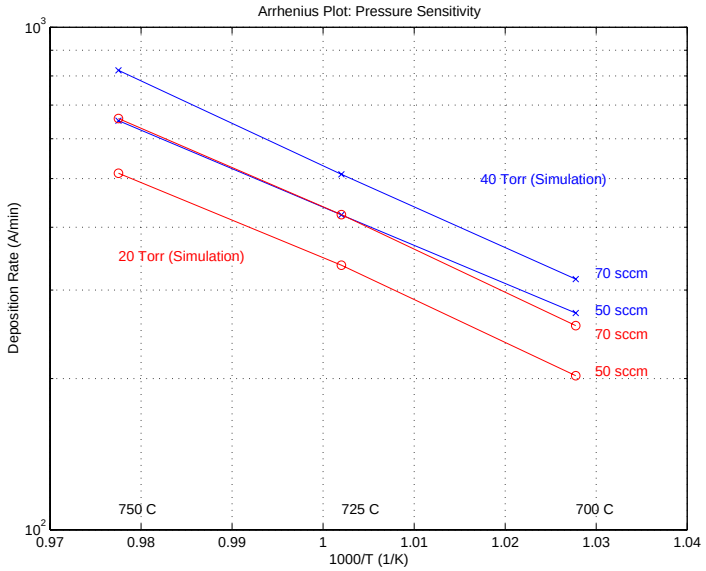

Figure 10: Plots illustrating Arrhenius relationship between poly-Si growth rate and wafer temperature in the Epsilon-1. Simulation data is taken for two silane flow rates (50, 70 sccm), three temperatures (700, 725, 750 C), and two chamber pressures (20, 40 Torr) . Growth rates for 40 Torr pressure are a factor of 1.26 times greater than growth rates for 20 Torr pressure consistently over the given range of temperatures and flow rates.

be approximately 0.5. This does not hold true (or come anywhere close) for our experimental and simulation data. However, we were able to determine an interesting relationship, by substituting silane flow rate F_{SiH_4} for flow velocity V in (26) and letting the power law exponent vary, i.e.,

$$R_{Si} = C F_{SiH_4}^{\alpha} \tag{27}$$

where α denotes the power law exponent, found by calculating the slope of $\log R_{Si}$ versus $\log F_{SiH_4}$. The log-log plots for experimental and simulation data over the range of temperatures we used are presented in Figure 11. The resulting values for α are given in Table 6. We see that the power law exponent α in (27) is roughly 0.7.

We also note that as the gas mixture flows through the process chamber, it heats up and consequently its density decreases and its velocity increases (see Section 5.3). This may partially account for the exponent being greater than 0.5.

Based on Equation (25), we also expect growth rate to be proportional to silane concentration and hence silane flow rate at the inlet. As shown in Figure 12, this relationship holds, with a temperature dependent proportionality constant, reflecting the fact that the process is thermally driven. This is in contrast to the temperature independent nature of the power law exponent. We emphasize that the power law is a purely mass transport controlled phenomenon.

5.1.4 Carrier Gas Sensitivity

A preliminary investigation of the relationship between growth rate and carrier gas was conducted by simulating poly-Si growth using N_2 carrier gas instead of H_2 carrier gas. Wafer temperature was set at 750 C and silane flow rate was set at 70 sccm. The resulting growth rate was 1661 A/min which is a factor of 2.5 times greater than the corresponding simulated growth rate using H_2 carrier.

These simulation results are in accordance with a study by Kleijn [12]. There, use of nitrogen results in an increase in buoyancy effects which causes an increase in the average residency time of gases in the reactor. Thus, gases are heated for a longer period of time and the contribution of gas phase reactions becomes greater. Also, thermal diffusion effects are weaker in nitrogen than in hydrogen. Both of these phenomena cause a larger growth rate in nitrogen than in hydrogen.

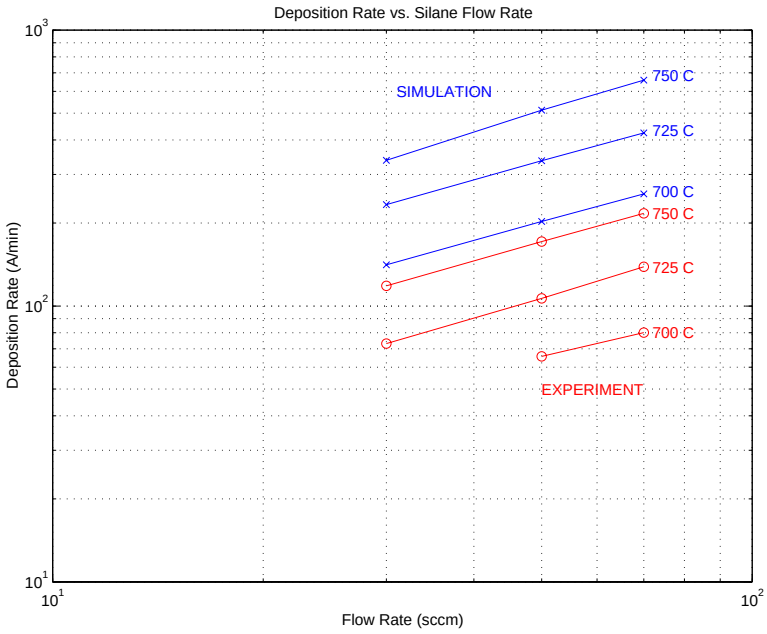

Figure 11: Plots illustrating power law relationship between poly-Si growth rate and silane flow rate in the Epsilon-1. Simulation and experimental data is taken for three silane flow rates (30, 50, 70 sccm) and three wafer temperatures (700, 725, 750 C). The power law exponent (slope of plots) is approximately 0.7, consistently over the given range of temperatures. The temperature independence of the power law exponent indicates a completely mass transport controlled phenomenon.

5.2 Deposition Uniformity Prediction

In Section 4.1, we presented an argument, based on anecdotal evidence, that temperature uniformity does not produce deposition thickness uniformity in the Epsilon-1 reactor, even for thermally activated processes. On the contrary, thermocouple offsets are set so that the temperature distribution on the wafer surface is intentionally non-uniform. This occurs because of the various transport phenomena that couple with thermally activated chemical mechanisms to influence silicon deposition rate in the Epsilon-1.

In this section we use simulation results to illustrate the phenomenon. We simulated poly-Si growth using 20 Torr chamber pressure, 750 C wafer temperature, 70 sccm silane flow rate, 20 slm H_2 carrier, and 7 slm H_2 purge. The 750 C temperature is uniform across the entire surface of the wafer. Figure 13 shows a contour plot of the resulting steady-state growth rate on the wafer surface.

Simulated growth rate varies from a minimum of 628 A/min at the downstream side to a maximum of 681 A/min at the upstream outer edge. This represents an 8.4% maximum variation in growth rate across the wafer surface. If thermal activation were the sole contributor to growth rate, then the 8.4% growth rate variation would correspond to a 0.42% maximum variation in temperature. However, we know this is not the case, since we have imposed a perfectly uniform temperature profile on the wafer. The existence of other contributing factors is apparent. On the other hand, this does show that compensation for the other factors may be achievable with much smaller thermocouples offsets than those currently used, which create a maximum temperature variation of 8.5% between thermocouple locations. The advantage to this would be reduced mechanical stress and a higher average temperature resulting in higher growth rates.

It is also worthwhile to examine the spatial distribution of the simulated growth rate non-uniformity. Growth rate appears to increase from wafer center to edges, and from front (upstream) side to rear (downstream) side. Thus, the expected depletion effect appears in poly-Si growth simulations. Non-uniformities in gas heating, resulting in non-uniform gas phase reactions and thermal diffusion may also be responsible for growth rate variations. Further simulations will be required to isolate those effects.

Thermocouple offset values described in Section 4.1 and used by Northrop Grumman to produce uniform growth create a temperature distribution that is hotter at the front (upstream) than the rear (downstream), and hotter at the

Relationship Between Growth Rate and Silane Flow Rate
Experiment vs. Simulation

Assumed Relationship
$R_{Si} = C F_{SiH_4}^{\alpha}$

Process Conditions	
Chamber Pressure	20 Torr
Carrier Gas	20 slm H_2
Source Gas	2% SiH_4 in H_2
Purge Gas	7 slm H_2

Symbol	Description	Experiment			Simulation		
T_w	Wafer Temperature (C)	700	725	750	700	725	750
α	Power Law Exponent		0.76	0.71	0.70	0.71	0.79

Table 6: Power law exponent calculated by fitting experimental and simulation data for poly-Si growth rate to an assumed power law relationship between growth rate and silane flow rate.

center than at the side. The latter seems to match what we would expect given our simulation results, i.e., cool the side to reduce growth rate there. On the other hand, it is difficult to explain the former, since it would exacerbate any reactant depletion effect. Perhaps the simulation understates the effect of downstream gas phase reactions.

We emphasize that in actual operation, the wafer is rotating, so that growth rate variations are averaged, and the significance of front-to-rear variations becomes unclear. We cannot draw any further conclusions at this time. A further experimental study of the effect of thermocouple offsets on uniformity is necessary.

5.3 Process Chamber Transport Phenomena Prediction

In this section we study the gas phase transport phenomena in the process chamber of the Epsilon-1. As stated earlier, these effects play an important role in determining deposition rate and uniformity for silicon growth. In particular, we want to observe and analyze gas flow patterns and non-uniformities in the spatial distribution of reactant species.

Simulation results described in this section are for poly-Si growth at 20 Torr pressure, 750 C uniform wafer temperature, 450 C chamber wall temperature, 70 sccm inlet silane flow rate, 20 slm hydrogen carrier flow rate, and 7 slm hydrogen purge flow rate.

We first examine the flow field in the process chamber. Gases are pumped into the Epsilon-1 process chamber from two inlets: the process gas inlet in the upper chamber section and the purge gas inlet in the lower chamber section. They are pumped out from the process chamber through one outlet located in the upper chamber section. Depending on process and purge inlet flow settings, it is possible for gases to flow from upper to lower chamber sections and visa-versa.

Figure 14 shows a view of the simulated flow field in the Epsilon-1 process chamber. Several features are of interest. We observe that there is no gas flow from the upper chamber through gaps to the lower chamber. Thus, the purge flow is effective in this regard. Also, gases from the lower chamber enter the upper chamber mainly through the gap toward the rear of the chamber and also somewhat through the gap near the side chamber wall. This causes the flow in the vicinity of the wafer to be directed from the side wall toward the center line of the chamber. In the *y*-direction, the flow takes a parabolic profile, i.e., slightly faster at the top of the chamber than near the wafer.

The contours in Figure 14 correspond to the flow speed in the *z*-direction, i.e., from front to rear. We observe that the gas velocity increases from front to rear. This is due to the fact that the gas heats up as it passes by the hot chamber walls and wafer level apparatus, causing the density of the gas mixture to decrease. However, differences in density do not cause any buoyancy driven recirculation cells in this simulation. This is because the flow velocity is relatively high and the temperature gradients in the hot wall chamber are not severe.

The heating of the gases is observed in Figure 15, which shows a contour plot of simulated temperature distribution in the Epsilon-1 process chamber. In the vicinity of the wafer the temperature increases from side to center and from wafer to chamber top wall, creating a highly non-uniform temperature field in the gas phase. We note that because the solid surfaces in the lower chamber section are also hot, the purge gas flowing up through the rear and side gaps does not cause a flow of cool gas to enter the upper chamber.

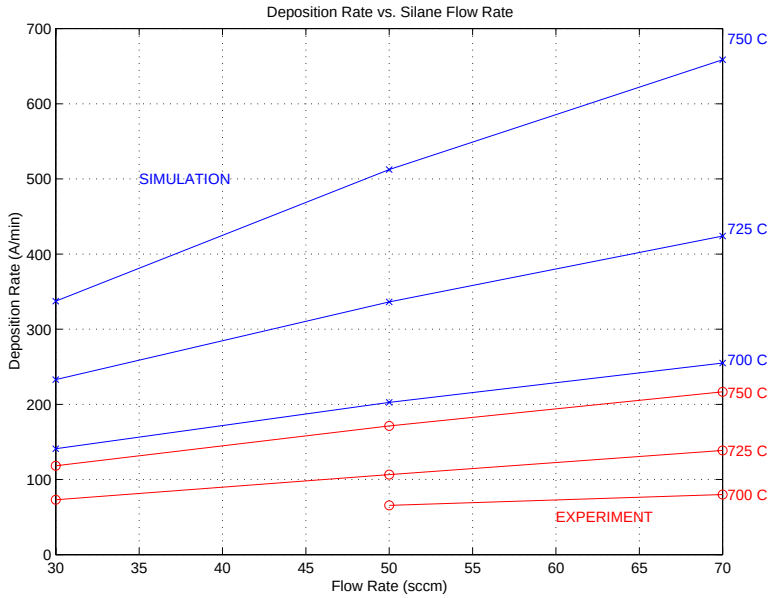

Figure 12: Plots illustrating linear relationship between poly-Si growth rate and silane flow rate in the Epsilon-1. Simulation and experimental data is taken for three silane flow rates (30, 50, 70 sccm) and three wafer temperatures (700, 725, 750 C). Slope of plots are temperature dependent, reflecting the fact that the process is thermally driven.

We now study the spatial distribution of the concentrations of the various reactant gases in the Epsilon-1. Silane enters the process chamber through the process inlet in the upper chamber section. It is also produced by one of the five gas phase reactions in the Kleijn model. The gas phase reactions also produce the reactive intermediaries: disilane, trisilane, silylsylene, and silylene. All of these gases are eventually diluted in the hydrogen carrier and hydrogen purge gas.

Figure 16 shows a contour plot of simulated silane mass fraction distribution. Silane mass fraction is a maximum at the inlet and becomes depleted by gas phase and surface reactions as the gas passes over the heated susceptor and wafer. It is at a minimum in locations where the hydrogen purge gas is flowing most heavily into the upper chamber section, in particular, at the side and rear of the ring.

The concentration distributions of the other reactive intermediaries are illustrated by contour plots in Figure 17. Because they do not enter at the inlet, these species appear in the flow only once the gas is hot enough for them to be produced, in this case at the front edge of the susceptor ring. Like silane, these species are depleted by surface reactions at the wafer surface. In fact, we observe that silylene, silylsylene, and trisilane are almost completely consumed by surface reactions. On the other hand, some disilane remains just above the wafer surface, although it is at a maximum in areas surrounding the wafer perimeter.

It is clear that the spatial distribution of reactant species concentrations is strongly influenced by the flow field, the gas phase temperature distribution, and surface reactions. We suggested earlier in this report that thermal diffusion may also play a role. This effect is more difficult to isolate and identify.

Figure 18 shows two contour plots: the top plot is for silane mass fraction and the bottom plot is for gas phase temperature. Both plots are snapshots of the $x-z$ plane approximately 2 mm above the wafer surface. In the area just above the wafer and susceptor, it is not possible to isolate any effect thermal diffusion may have, i.e., separate it from the depletion effect caused by gas phase and surface reactions. However, if we restrict attention to the area between the side ring-shelf gap and the side chamber wall, we observe a silane mass fraction gradient that may be due to the Soret effect. In particular, silane mass fraction increases steadily along the chamber side wall and side ring-shelf gap from front to rear. It is possible that the relatively heavy silane molecules have diffused toward the cooler area near the chamber side wall at the front ring-shelf gap and away from the hotter area toward the rear. Again, we emphasize that this speculation needs to be confirmed by conducting additional simulations and possibly actual experiments.

We also note that simulation results show no diffusion of silane or other reactive intermediaries into the lower chamber section. Evidently, the convective forces of the gas flow dominate through the gaps so that any heavy molecules diffusing toward the lower chamber are immediately swept back into the upper chamber.

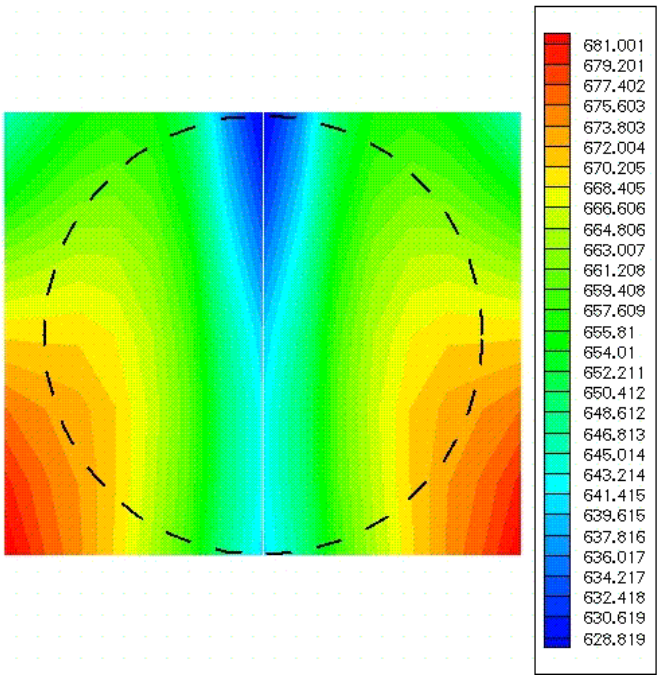

Figure 13: Spatial distribution of steady-state deposition rate (A/min) on wafer surface resulting from poly-Si growth with 750 C uniform temperature. The picture shows a non-uniform deposition rate despite the uniform temperature profile. Process conditions are 20 Torr pressure and 70 sccm silane flow rate. Gas flow is from bottom of picture (front/upstream) to top of picture (rear/downstream).

5.4 Purge Flow Optimization

As we observed in Section 5.3, the 7 slm H_2 purge flow is effective in preventing any source gases from entering the lower chamber section. In particular, the mass fractions of silane and other reactive intermediaries in the lower chamber were zero for those simulations. This motivates an examination of the relationship between purge flow rate, reactant concentrations in the lower chamber, and possible deposition on the back-side of the susceptor. The objective is to optimize purge flow rate, where the cost to be minimized is proportional to the amount of consumed H_2, and any back-side deposition is unacceptable.

Figure 19 shows contours of silane mass fraction and flow streamlines resulting from two simulations, each using a different H_2 purge flow rate. The top and bottom figures correspond to 7 slm and 2 slm H_2 purge flow rates, respectively. We observe that purge flow rate has an effect on both the flow pattern in the process chamber and the distribution of reactant concentrations. For the 7 slm simulation, steady-state silane concentration in the lower chamber is zero, and streamlines indicate a regular smooth flow from inlets to outlet, with purge gases entering the upper chamber mainly through the rear ring-shelf gap. For the 2 slm simulation, silane concentration in the lower chamber is nonzero, and the flow field becomes irregular, including mixing between upper and lower chambers and recirculation cells in the lower chamber.

For the above simulations, we modeled both the front-side of the wafer and the back-side of the susceptor as reacting surfaces. We note that the wafer and susceptor have different material properties, but we modeled the back-side of the susceptor as if it were the back-side of a silicon wafer. Process conditions were set to 20 Torr pressure, 750 C wafer temperature, and 70 sccm silane flow rate at the upper chamber inlet. For the 7 slm purge flow simulation, no back-side deposition occurred, and average front-side deposition rate was 687 A/min. For the 2 slm purge flow simulation, back-side deposition rate varied from 205 to 359 A/min across the susceptor back-side surface, and average front-side deposition rate was 719 A/min. Apparently, the different flow pattern resulting from a reduction in purge flow rate also causes the front-side deposition rate to increase.

For purposes of optimization we performed one additional simulation with a 5 slm H_2 purge flow. Results qualitatively matched those for the 7 slm purge simulation, i.e., no back-side deposition and zero silane concentration in the

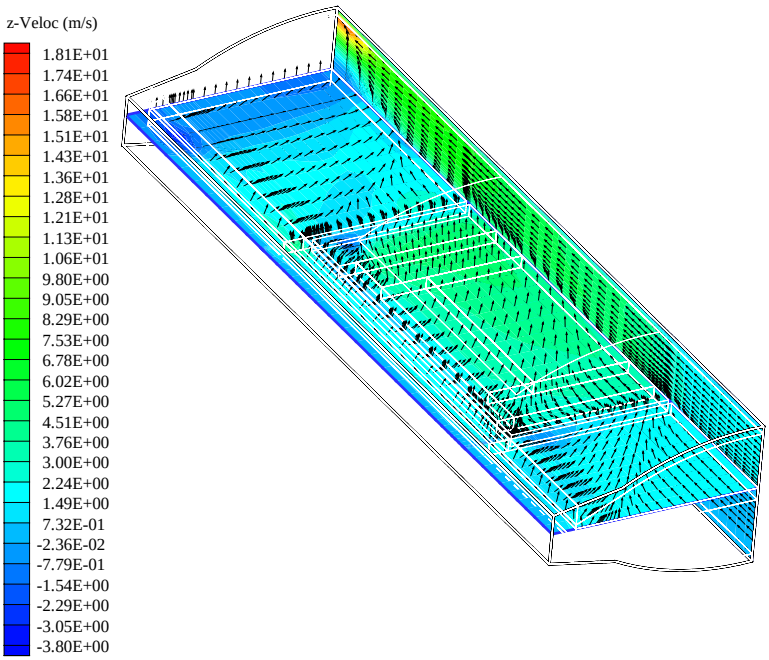

Figure 14: Steady state flow pattern of gases in the Epsilon-1 process chamber. Process conditions are 20 slm hydrogen carrier, 70 sccm silane source, 750 C wafer temperature, 450 C chamber wall temperature, and 20 Torr pressure.

lower chamber section. Based on simulation results, we can reduce the flow rate of H_2 purge from 7 slm to 5 slm, thus reducing the use of consumable gases while still maintaining purge effectiveness. However, a reduction to 2 slm is too much and results in unacceptable back-side deposition. The optimum purge flow rate is somewhere between 2 slm and 5 slm. We did not proceed further with this study.

5.5 Injector Flow Analysis

As described in Section 4.4, a 3-dimensional finite volume mesh was developed for modeling flow through the injector apparatus and inlet flange into the process chamber. The goal here is to investigate the effect of inlet flow velocity and injector settings on the fully developed chamber flow. We present only a partial analysis.

Figure 20 shows the flow field resulting from injection of a 1.4 m/sec flow through the three injector slits, each of which is set to a 0.010 inch width. The 1.4 m/sec flow velocity corresponds to process flow rates of 30 sccm silane source and 20 slm hydrogen carrier. Flow through the injector apparatus is downward through the slits until it hits the bottom of the inlet flange, at which point it is forced to change direction toward the chamber entrance. We observe that after striking the bottom, the flow profile is irregular, but smoothes out to a relatively uniform profile before it reaches the ring and susceptor.

This model can be used to study the effect of injector slit widths on the flow profile in the chamber. Due to time constraints and the imminent replacement of gas injection equipment, we deferred this study to future work. In addition, since Northrop Grumman performs some experiments with high flow rates, it would be useful to investigate the limits on flow velocity for achieving a regular and relatively uniform flow across the ring and susceptor.

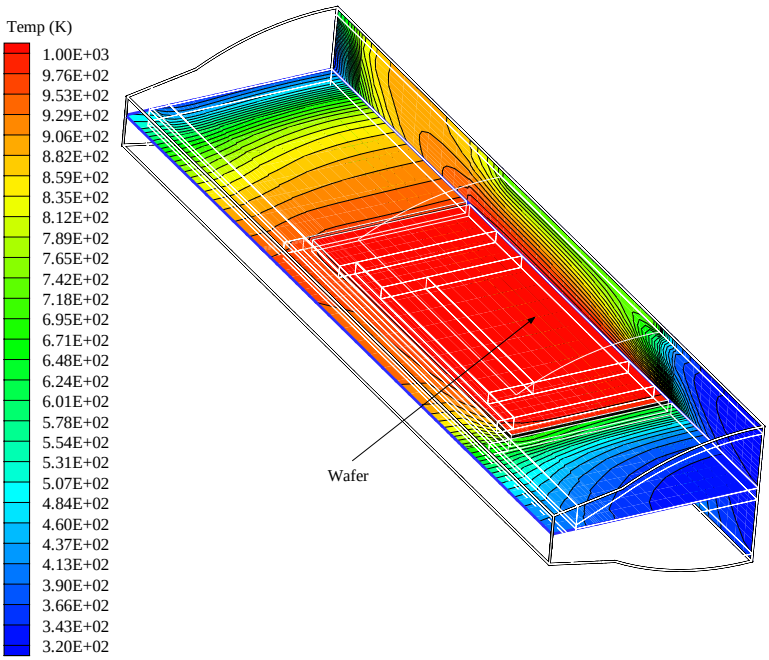

Figure 15: Cross-sectional view of the steady-state gas phase temperature distribution in the ASM Epsilon-1 process chamber during growth of poly-Si. Process conditions are 750 C wafer temperature, 450 C chamber wall temperature, 20 slm hydrogen carrier, 70 sccm silane source, and 20 Torr pressure .

6 Conclusions

We have presented strong anecdotal evidence, based on thermocouple offsets used by Northrop Grumman to produce uniform silicon growth in the Epsilon-1 reactor, that gas phase transport phenomena play an important role in determining deposition uniformity, even for thermally activated growth. This conjecture is in agreement with a study by Kleijn [12] using simulation and experimental data for silicon growth in a cold-wall cylindrical reactor. Initial models for silicon growth in the Epsilon-1 presented in [21] cannot be coupled to gas phase transport phenomena and use a simplified chemical kinetics model. This motivated the development of a 3-dimensional comprehensive process-equipment model for silicon growth in the Epsilon-1, incorporating as many relevant transport effects and chemical mechanisms as was feasible from a practical standpoint.

The process-equipment model provides a tool for prediction of deposition rate and other process variables, i.e., the process-equipment state, for a given set of recipe inputs (process conditions) and equipment settings. The predictive capability of the model was tested by comparing results of poly-Si growth simulations to experimental data. Simulations predict growth rates that are roughly three times greater than actual growth rates, consistently over the given range of operating conditions.

Using the process-equipment model, we performed simulations in order to study the factors that influence deposition rate and uniformity for silicon growth in the Epsilon-1. The relationship between poly-Si growth rate and wafer temperature, chamber pressure, silane flow rate, and hydrogen carrier flow rate were investigated. Although we used a complicated model for poly-Si growth mechanisms developed by Kleijn [12], growth rate temperature sensitivity can be simplified to an Arrhenius relationship. Simulation results indicate that growth rate increases with the logarithm (base 10) of chamber pressure, in agreement with known relationships. We found a power law relationship connecting poly-Si growth rate with silane flow rate at the inlet, with power law exponent roughly 0.7. Finally, we demonstrated that substitution of nitrogen for hydrogen as the carrier gas results in a significantly increased deposition rate.

Simulation results showed that temperature uniformity does not guarantee deposition uniformity in the Epsilon-1. Simulations using a uniform wafer temperature in the thermally activated regime produced growth rates that were non-uniform across the wafer surface. Thus, it is apparent that achieving deposition uniformity requires some degree of temperature non-uniformity to compensate for the effects of other phenomena including reactant depletion, gas

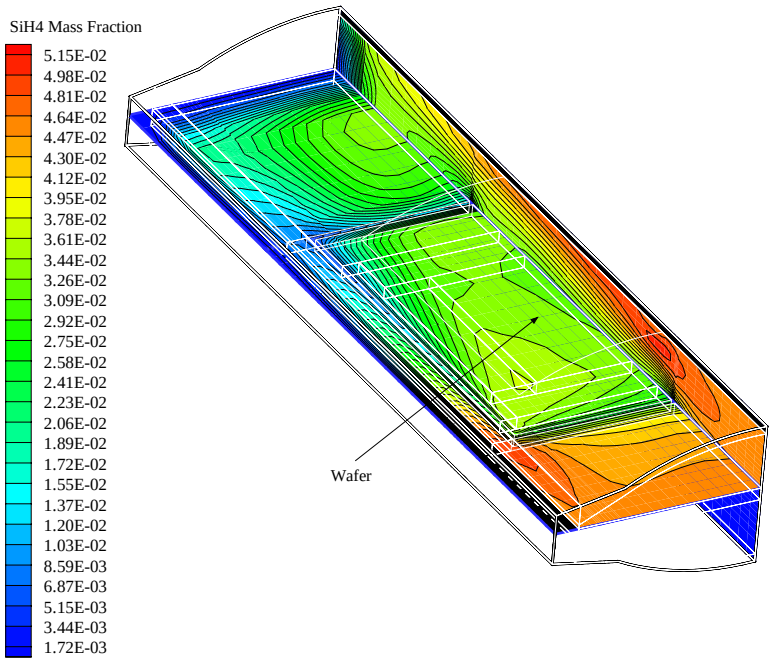

Figure 16: Steady-state silane mass fraction distribution in the Epsilon-1 process chamber during poly-Si growth. Process conditions are 750 C wafer temperature, 450 C chamber wall temperature, 20 slm hydrogen carrier, 70 sccm silane source, and 20 Torr pressure .

heating and gas phase reactions, thermal diffusion of species, and flow patterns.

7 Acknowledgements

The authors are grateful for the assistance and contributions of colleagues at Northrop Grumman ESSS, Baltimore, MD, and ASM America, Inc., Phoenix, AZ. The authors are indebted to Mr. Sam Ponczak of Northrop Grumman for financial support as well as project motivation and his continual support and commentary. Mr. Paul Brabant of Northrop Grumman and Mr. Andrew Newman performed the growth and lamp heating experiments at Northrop Grumman ESSS. In addition, Mr. Brabant supplied a great deal of information about the reactor and its operation including results of previous experiments and production runs. His involvement with this project has been indispensable. Dr. Thomas Knight and Dr. Michael O'Loughlin of Northrop Grumman provided a broad range of useful analysis and commentary. The authors also thank Dr. Douglas Meyer of ASM America for his analysis and comments regarding process and equipment details and physics. The authors are especially grateful to Dr. Meyer, Mr. Tony Komasa, Mr. Rod Smith, and co-workers at ASM America who provided the authors with invaluable tours, demonstrations, and detailed information about the Epsilon-1. Finally, we offer thanks to Prof. Howard Stone of Harvard University Division of Engineering and Applied Sciences for his comments regarding dimensional analysis and the relationship between growth rate and flow rates.

References

[1] Stephen A. Campbell. Rapid thermal processing. In M. Meyyappan, editor, *Computational Modeling in Semiconductor Processing*, chapter 6, pages 325–350. Artech House, 1995.

[2] Chatterjee, Trachtenberg, and Edgar. Modeling of a single wafer rapid thermal reactor. *Journal of the Electrochemical Society*, 139:3682–3689, December 1992.

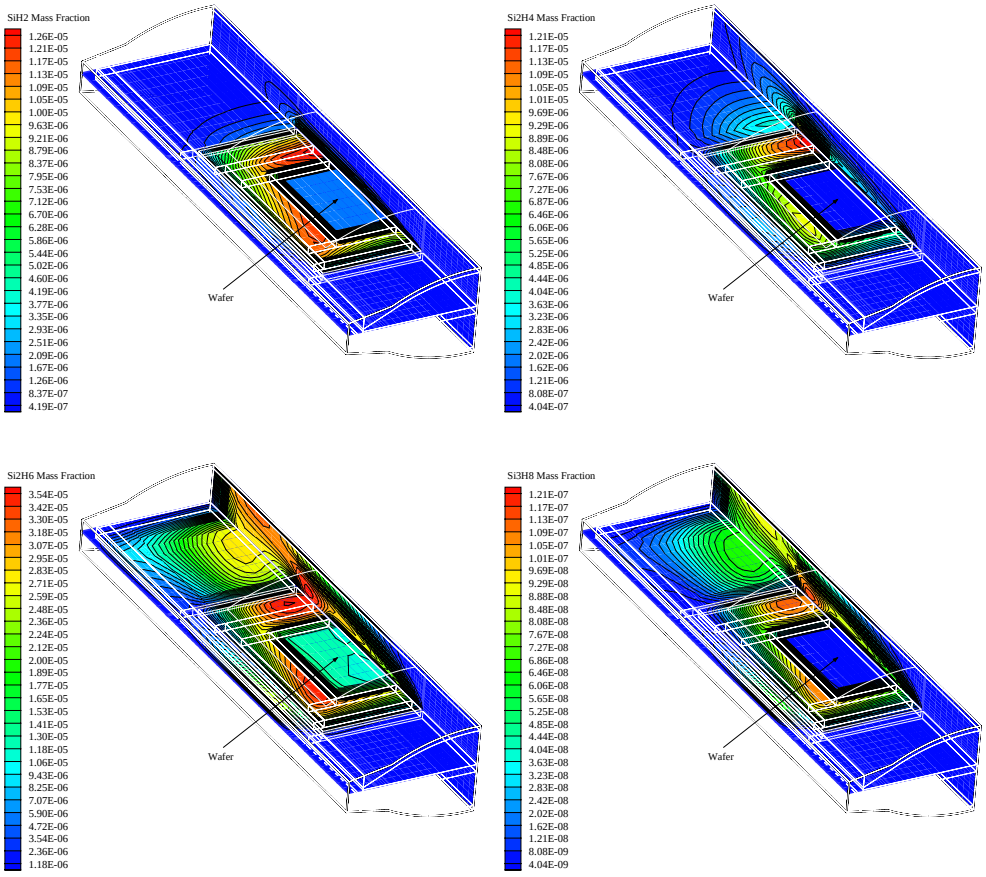

Figure 17: Steady-state mass fraction distribution for reactive intermediaries during poly-Si growth: silylene (top-left), silylsylene (top-right), disilane (bottom-left), trisilane (bottom-right). Process conditions are 750 C wafer temperature, 450 C chamber wall temperature, 20 slm hydrogen carrier, 70 sccm silane source, and 20 Torr pressure .

[3] Y.M. Cho and T. Kailath. Model identification in RTP systems. *IEEE Transactions on Semiconductor Manufacturing*, 6(3):233–245, August 1993.

[4] Young Man Cho and Paul Gyugyi. Control of rapid thermal processing: A system theoretic approach. *IEEE Transactions on Control Systems Technology*, 5(6):644653, November 1997.

[5] M. E. Coltrin, R. J. Kee, and J. A. Miller. *Journal of the Electrochemical Society*, 133:1206, 1986.

[6] W.B. de Boer and D.J. Meyer. Low temperature CVD of epitaxial Si and Si–Ge layers at atmospheric pressure. *Applied Physics Letters*, 58(12):1286–1288, March 1991.

[7] Dimitrios I. Fotiadis, Shigekazu Kieda, and Klavs F. Jensen. Transport phenomena in vertical reactors for metalorganic vapor phase epitaxy: 1. Effects of heat transfer characteristics, reactor geometry, and operating conditions. *Journal of Crystal Growth*, 102:441–470, 1990.

[8] R.S. Gyurcsik, T.J. Riley, and F. Y. Sorrell. A model for rapid thermal processing: Achieving uniformity through lamp control. *IEEE Transactions on Semiconductor Manufacturing*, 4(1):9–13, February 1991.

[9] T.I. Kamins and D.J. Meyer. Kinetics of Si–Ge deposition by APCVD. *Applied Physics Letters*, 59(2):90, July 1991.

[10] T.I. Kamins and D.J. Meyer. Effect of silicon source gas on silicon-germanium chemical vapor deposition kinetics at atmospheric pressure. *Applied Physics Letters*, 61(1):90, July 1992.

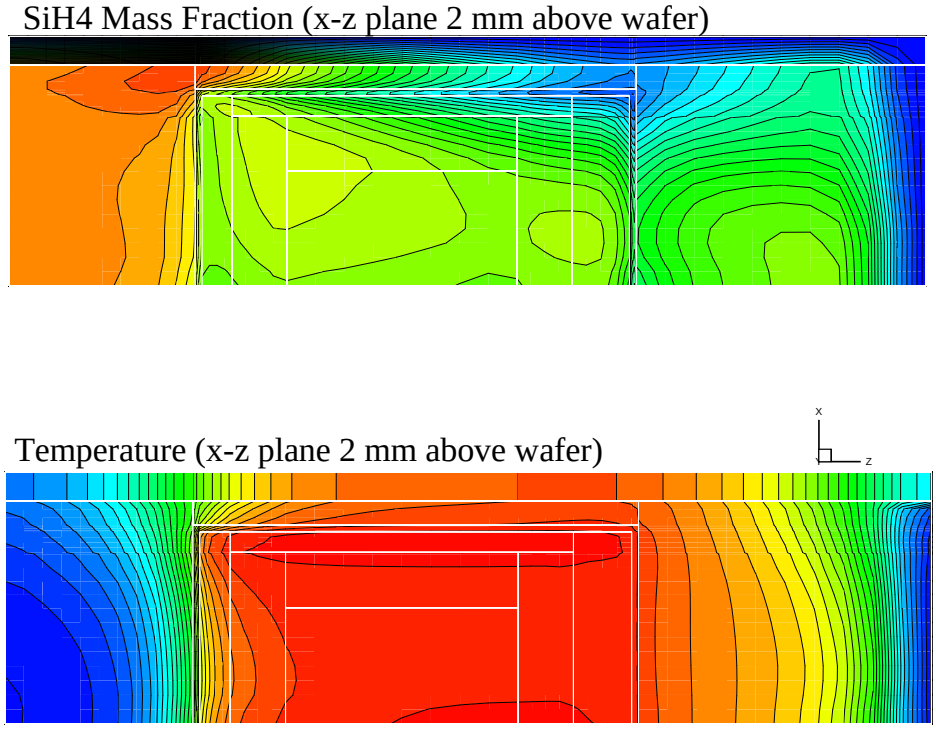

Figure 18: Illustration of thermal diffusion (Soret effect) in the Epsilon-1 process chamber. Contours of steady-state silane mass fraction (top) and temperature (bottom) for the $x-z$ plane approximately 2 mm above the wafer surface.

[11] A. Kersch. RTP reactor simulations. *The PHOENICS Journal of Computational Fluid Dynamics and its Applications*, 8(4):500–511, dec 1995.

[12] C. R. Kleijn. A mathematical model of the hydrodynamics and gas–phase reactions in silicon LPCVD in a single–wafer reactor. *Journal of the Electrochemical Society*, 138(7):2190–2200, July 1991.

[13] C. R. Kleijn and K. J. Kuijlaars. The modelling of transport phenomena in CVD reactors. *The PHOENICS Journal of Computational Fluid Dynamics and its Applications*, 8(4):404–420, December 1995.

[14] C.R. Kleijn. Chemical vapor deposition processes. In M. Meyyappan, editor, *Computational Modeling in Semiconductor Processing*, chapter 4, pages 97–229. Artech House, 1995.

[15] Karson L. Knutson, Stephen A. Campbell, and Floyd Dunn. Modeling of three–dimensional effects on temperature uniformity in rapid thermal processing of eight inch wafers. *IEEE Transactions on Semiconductor Manufacturing*, 7(1):68–72, February 1994.

[16] M. Liehr, C. M. Greenlief, S. R. Kasi, and M. Offenberg. Kinetics of silicon epitaxy using sih_4 in a rapid thermal chemical vapor deposition reactor. *Applied Physics Letters*, 56(7):629–631, February 1990.

[17] Guangquan Lu, Monalisa Bora, Laura L. Tedder, and Gary W. Rubloff. Integrated dynamic simulation of rapid thermal chemical vapor deposition of polysilicon. *IEEE Transactions on Semiconductor Manufacturing*, 11(1):63–74, February 1998.

[18] Douglas Meyer, Tony Komasa, and Rod Smith. Private communication. ASM America, Inc., Phoenix, AZ, April 1998.

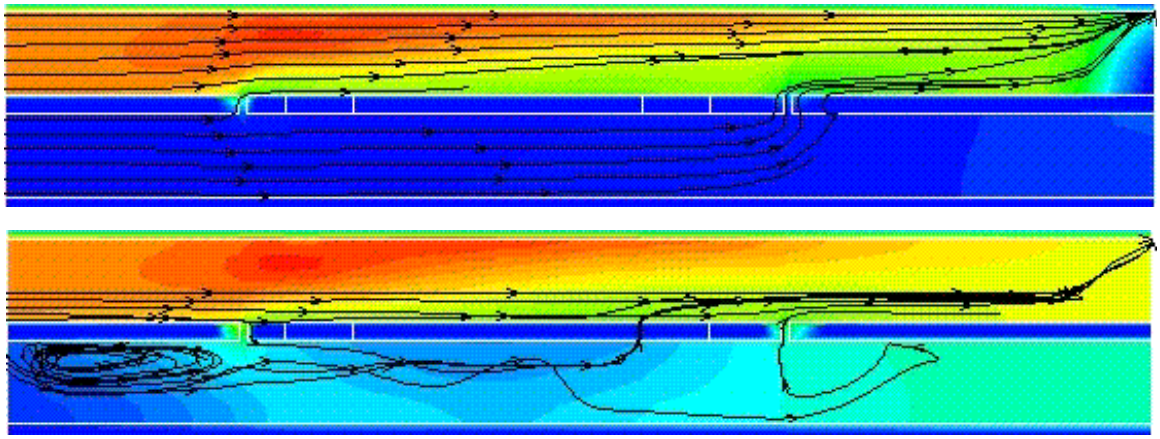

Figure 19: Comparison of flow streamlines and steady-state silane mass fraction contours for hydrogen purge flow rates of 7 slm (top) and 2 slm (bottom). The higher purge flow rate results in zero silane concentration in the lower chamber section, no back-side deposition, and regular flow from inlets to outlet. The lower purge flow rate is ineffective, producing non-zero silane concentration in the lower chamber section and some back-side deposition.

[19] Meyya Meyyappan. Various private communications. NASA Ames, October–March 1998–1999.

[20] Andrew Newman, P.S. Krishnaprasad, Sam Ponczak, and Paul Brabant. Modeling and model reduction for epitaxial growth. In *Proceedings of the SEMATECH AEC/APC Workshop IX*. SEMATECH, September 1997.

[21] Andrew Newman, P.S. Krishnaprasad, Sam Ponczak, and Paul Brabant. Modeling and model reduction for control and optimization of epitaxial growth in a commercial RTCVD reactor. Technical Report 98-45, Institute for Systems Research, 1998.

[22] Andrew J. Newman and P. S. Krishnaprasad. Nonlinear model reduction for rtcvd. In *Proceedings of the 32nd Conference on Information Sciences and Systems*, Princeton, NJ, 1998.

[23] Sam Ponczak, Thomas Knight, Michael O'Loughlin, and Paul Brabant. Various private communications. Northrop Grumman ESSS, Linthicum, MD, March–October 1998.

[24] W. R. Runyan and K. E. Bean. *Semiconductor Integrated Circuit Processing Technology*, chapter 7, pages 294–360. Addison-Wesley, 1990.

[25] Charles Schaper and Thomas Kailath. Thermal model validation for RTCVD of polysilicon. *Journal of the Electrochemical Society*, 143(1):374–381, January 1996.

[26] F. Y. Sorrell, M. J. Fordham, M. C. Ozturk, and J. J. Wortman. Temperature uniformity in RTP furnaces. *IEEE Transactions on Electron Devices*, 39(1):75–79, January 1992.

[27] F. Yates Sorrell, Seungil Yu, and William J. Kiether. Applied RTP optical modeling: An argument for model-based control. *IEEE Transactions on Semiconductor Manufacturing*, 7(4):454–459, November 1994.

[28] S.M. Sze. *Physics of Semiconductor Devices*. Wiley Interscience, 1981.

[29] Chr. Werner and M. Hierlemann. Application of PHOENICS–CVD to epitaxial Si–Ge, polysilicon, and silicon deposition in a range of CVD reactors. *The PHOENICS Journal of Computational Fluid Dynamics and its Applications*, 8(4):538–552, December 1995.

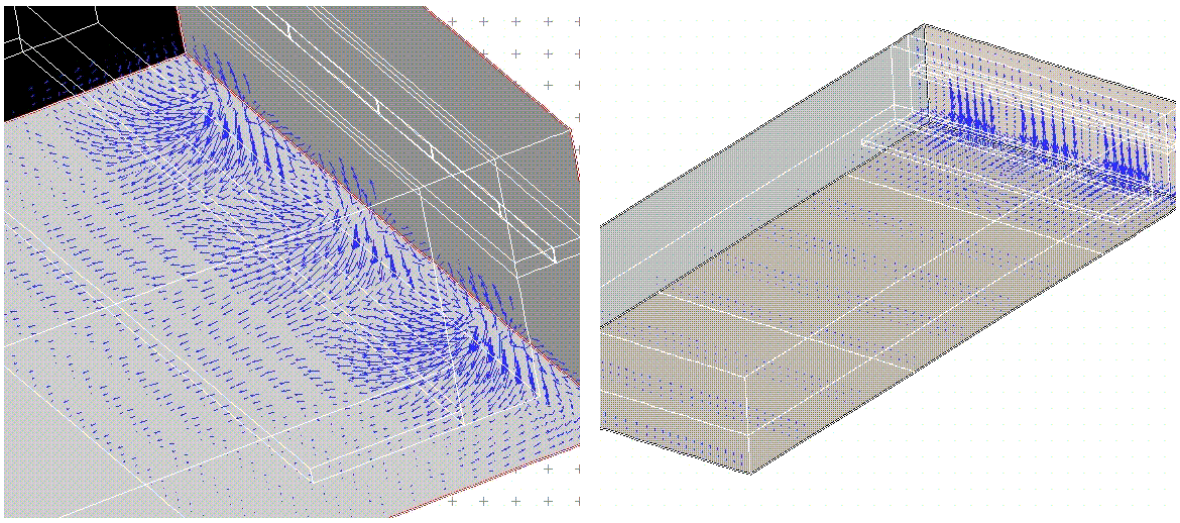

Figure 20: Steady state flow of gases into and through the injector; close-up (left) and broader view (right). Flow is downward through three injector slits, each set at 0.010 inch width. Flow hits bottom and changes direction toward chamber entrance. Flow becomes regular relatively soon after entering chamber.